Preprint typeset using LaTeX style emulateapj v. 08/13/06

SYSTEMATIC NLTE STUDY OF THE $-2.6 \leq$ [FE/H] ≤ 0.2 F AND G DWARFS IN THE SOLAR NEIGHBOURHOOD. I. STELLAR ATMOSPHERE PARAMETERS

T. Sitnova
Key Laboratory of Optical Astronomy, National Astronomical Observatories, Chinese Academy of Sciences, Beijing 100012, China
Institute of Astronomy, Russian Academy of Sciences, RU-119017 Moscow, Russia and
Lomonosov Moscow State University, RU-119991 Moscow, Russia

G. Zhao
Key Laboratory of Optical Astronomy, National Astronomical Observatories, Chinese Academy of Sciences, Beijing 100012, China

L. Mashonkina
Institute of Astronomy, Russian Academy of Sciences, RU-119017 Moscow, Russia

Y. Chen
Key Laboratory of Optical Astronomy, National Astronomical Observatories, Chinese Academy of Sciences, Beijing 100012, China

F. Liu
Key Laboratory of Optical Astronomy, National Astronomical Observatories, Chinese Academy of Sciences, Beijing 100012, China and
Research School of Astronomy and Astrophysics, Australian National University, Canberra, ACT 2611, Australia

Yu. Pakhomov
Institute of Astronomy, Russian Academy of Sciences, RU-119017 Moscow, Russia

K. Tan
Key Laboratory of Optical Astronomy, National Astronomical Observatories, Chinese Academy of Sciences, Beijing 100012, China

M. Bolte
UCO/Lick Observatory, University of California, 1156 High St., Santa Cruz, CA 95064, USA

S. Alexeeva
Institute of Astronomy, Russian Academy of Sciences, RU-119017 Moscow, Russia

F. Grupp
Universitats Sternwarte Munchen, Scheinerstr. 1, D-81679 Munchen, Germany and
Max-Planck-Institut fur extraterrestrische Physik, Giessenbachstrasse, D-85748 Garching, Germany

J.-R. Shi
Key Laboratory of Optical Astronomy, National Astronomical Observatories, Chinese Academy of Sciences, Beijing 100012, China

H.-W. Zhang
Department of Astronomy, School of Physics, Peking University, Beijing 100871, PR China

ABSTRACT

We present atmospheric parameters for 51 nearby F and G dwarf and subgiant stars uniformly distributed over the $-2.60 <$ [Fe/H] $< +0.20$ metallicity range that is suitable for the Galactic chemical evolution research. Lines of iron in the two ionization stages, Fe I and Fe II, were used to derive a homogeneous set of effective temperatures, surface gravities, iron abundances, and microturbulence velocities. Our spectroscopic analyses took advantage of employing high-resolution ($R \geq 60\,000$) Shane/Hamilton and CFHT/ESPaDOnS observed spectra and non-local thermodynamic equilibrium (NLTE) line formation for Fe I and Fe II in the classical 1D model atmospheres. The spectroscopic method was tested in advance with the 20 benchmark stars, for which there are multiple measurements of the infrared flux method (IRFM) effective temperature and their Hipparcos parallax error is less than 10 %. We found NLTE abundances from lines of Fe I and Fe II to be consistent within 0.06 dex for every benchmark star, when applying a scaling factor of $S_{\rm H} = 0.5$ to the Drawinian rates

of inelastic Fe+H collisions. The obtained atmospheric parameters were checked for each program star by comparing its position in the log g – $T_{\rm eff}$ plane with the theoretical evolutionary track of given metallicity and α-enhancement in the Yi et al. (2004) grid. Our final effective temperatures lie exactly in between the $T_{\rm IRFM}$ scales of Alonso et al. (1996a) and Casagrande et al. (2011), with a mean difference of +46 K and −51 K, respectively. NLTE leads to higher surface gravity compared with that for LTE. The shift in log g is smaller than 0.1 dex for stars with either [Fe/H] ≥ -0.75, or $T_{\rm eff} \leq 5750$ K, or log g ≥ 4.20. NLTE analysis is crucial for the VMP turn-off and subgiant stars, for which the shift in log g between NLTE and LTE can be up to 0.5 dex. The obtained accurate atmospheric parameters will be used in the forthcoming papers to determine NLTE abundances of important astrophysical elements from lithium to europium and to improve observational constraints on the chemo-dynamical models of the Galaxy evolution.

Subject headings: Stars: abundances – Stars: atmospheres – Stars: fundamental parameters

1. INTRODUCTION

In recent decades the construction of large telescopes, the developement of efficient spectrometers, and progress in stellar atmosphere and synthetic spectrum numerical modelling provided a considerable improvement in the quality and quantity of stellar abundance determinations. Elemental abundances for the FGK-type stars provide important clues to understand the main processes at play in formation and evolution of the Milky Way (MW). Studies of stellar samples with metallicity [Fe/H][1] ≥ -1 showed how trends in various chemical elements can be used to learn the chemodynamical evolution of the Galactic disk (Edvardsson et al. 1993; Chen et al. 2000) and to resolve the thick disk and thin disk (Gratton et al. 1996; Fuhrmann 1998, 2004; Mashonkina & Gehren 2000; Reddy et al. 2003; Mishenina et al. 2004; Zhang & Zhao 2006; Adibekyan et al. 2013; Bensby et al. 2014, and references therein). Studies of very metal-poor (VMP, [Fe/H] ≤ -2) stars unraveled the major processes of chemical enrichment of the Milky Way (McWilliam et al. 1995; Cayrel et al. 2004; Zhang & Zhao 2005; Bonifacio et al. 2009).

Elemental abundances of stars with different metallicities are the main constraint for Galactic chemodynamical models (e.g. Chiappini et al. (2001); Romano et al. (2010); Kobayashi et al. (2011)). For the Galactic chemical evolution research it would be useful to deal with a homogeneous set of accurate stellar abundances in wide metallicity range, from supersolar down to extremely low iron abundances. Large high-resolution spectroscopic surveys were proposed to increase the statistics of observations and to improve a homogeneity of derived stellar chemical abundances over wide metallicity range. The Apache Point Observatory Galactic Evolution Experiment (APOGEE) (Zasowski et al. 2013), with its 10^5 red giants observed in the near-infrared H-band with a spectral resolving power of $R \simeq 22\,500$, enables users to address numerous Galactic structure and stellar populations issues. The Gaia-ESO Survey consortium (Gilmore et al. 2012; Randich et al. 2013; Smiljanic et al. 2014) is obtaining high-quality spectroscopic data for about 10^5 stars using FLAMES at the VLT. Spectra for a million stars will be acquired by the coming Galactic Archaeology with HERMES (GALAH) survey (De Silva et al. 2015).

We initiate a new project of deriving a homogeneous set of stellar atmosphere parameters and chemical abundances for the Galactic field FGK-type stars in the metallicity range $-3 \leq$ [Fe/H] $\leq +0.3$ that is suitable for a systematic research of Galactic chemical evolution. By employing high-resolution spectral observations, deriving accurate stellar atmosphere parameters, and treating the non-local thermodynamic equilibrium (NLTE) line formation for the key chemical species, we attempt to push the accuracy of the abundance analysis to the points where the trends with metallicity could be meaningfully discussed. The selected stars are uniformly distributed in metallicity and they can serve as a calibration sample for the existing and coming large-scale stellar surveys, such as the LAMOST Experiment for Galactic Understanding and Exploration (LEGUE Deng et al. 2012), designed to determine from low-resolution spectra elemental abundances for hundreds of thousands to millions of stars, spread over much larger distances than ever before.

The goal of the present paper is the determination of precise atmospheric parameters, i.e. the effective temperature, $T_{\rm eff}$, the surface gravity, log g, the iron abundance, [Fe/H], and the microturbulence velocity, ξ_t, for the selected sample of, presumably, dwarf stars. The next papers in the series will concern with calculations of the NLTE abundances for many chemical elements from Li to Eu and analysis of the obtained abundance trends. Taking advantage of the Shane/Hamilton and CFHT/ESPaDOnS high-resolution observational material with sufficient spectral coverage and the NLTE line formation for Fe I-Fe II, we determined stellar atmosphere parameters spectroscopically from lines of iron in the two ionization stages, Fe I and Fe II.

The spectroscopic methods are, in particular, useful for evaluating $T_{\rm eff}$ and log g of the VMP stars that are mostly distant, and, therefore, their temperatures cannot be reliably derived from photometric colours due to the uncertainty in the interstellar reddening data and, at present, surface gravities cannot be calculated from the trigonometric parallax because it is either rather uncertain or non-measurable. We look forward to seeing soon accurate parallaxes from Gaia[2]. In the literature there is no consensus on a validity of the excitation temperatures, $T_{\rm exc}$, derived through forcing no dependence of the Fe I line abundance on the excitation energy of the lower level, $E_{\rm exc}$. For their sample of VMP cool giants Cayrel et al. (2004) reached in LTE good agreement between the photometric and spectroscopic tem-

Electronic address: sitnova@inasan.ru

[1] In the classical notation, where [X/H] = $\log(N_{\rm X}/N_{\rm H})_{star} - \log(N_{\rm X}/N_{\rm H})_{Sun}$.

[2] `http://sci.esa.int/gaia/`

peratures after they excluded strong lines with $E_{\rm exc} = 0$ eV. A similar approach (LTE, but not cutting $E_{\rm exc} = 0$ eV) yielded the same outcome for the VMP near-main-sequence stars in Frebel et al. (2013), while up to several hundred degrees cooler excitation temperatures than the photometric ones were found for the cool giants.

Ruchti et al. (2013) determined surface gravities of the stellar sample selected from the RAVE survey, using a grid of the NLTE abundance corrections from Lind et al. (2012). For common $T_{\rm eff}$ in the NLTE and LTE analysis, they found systematic biases in log g of up to 0.2 dex in the metallicity range $-2 <$ [Fe/H] < -0.5 and up to 0.3 dex for the more metal-poor stars.

The NLTE effects for lines of Fe I were accounted for by Bensby et al. (2014) in their study of 714 F and G dwarf stars, by applying the NLTE abundance corrections interpolated in the grid of Lind et al. (2012). They found minor shifts between NLTE and LTE, with $\Delta T_{\rm eff} = -12 \pm 28$ K, Δlog g $= +0.012 \pm 0.059$, and $\Delta \log \varepsilon$(Fe) $= -0.013 \pm 0.016$, on average. This is because the majority of their stars are close-to-solar metallicity and mildly metal-deficient ones, with [Fe/H] > -1.2, and the NLTE abundance corrections are small, at the level of few units of hundredth, as predicted by Mashonkina et al. (2011) and Lind et al. (2012) for this metallicity range. Furthermore, the NLTE calculations of Lind et al. (2012) resulted in small departures from LTE for Fe I until the extremely low metallicities because they were performed assuming a high efficiency of the Fe+H collisions and using the Drawinian rates (Drawin 1968, 1969). For nearby stars with very good Hipparcos parallaxes ($\Delta\pi/\pi < 0.05$), Bensby et al. (2014) found that essentially all stars with log g > 4.2 and $T_{\rm eff} < 5650$ K do not show ionization equilibrium between Fe I and Fe II, when determining the surface gravity from Hipparcos parallaxes. Bensby et al. (2014) suggested that classical plane-parallel (1D) models have limitations and cannot properly handle excitation balance and/or ionization balance, and they applied, therefore, empirical corrections to the atmospheric parameters from ionization balance. In this study we check with our stellar sample, whether spectroscopic methods of $T_{\rm eff}$ and log g determination from lines of Fe I and Fe II have any limitations and what they are.

The paper is structured as follows. In Sect. 2 we describe the stellar sample, observations, and their reduction. Kinematical properties of the selected stars are calculated in Sect. 3. They are used to identify a membership of individual stars to the galactic stellar populations. Section 4 concerns with the methodical issues. Stellar effective temperatures, surface gravities, iron abundances, microturbulence velocities, and masses are derived in Sect. 5. The obtained results are discussed in Sect. 6. Our conclusions are presented in Sect. 7.

2. STELLAR SAMPLE, OBSERVATIONS, SPECTRA REDUCTION

The stars were selected from the [Fe/H] catalogue of Cayrel de Strobel et al. (2001) based on the following criteria.

1. The stars have a declination of $\delta > -20^\circ$ to be observed at the nothern sky.

2. The selected stars should cover as broad as possible metallicity range and be uniformly distributed, with 2-3 stars in each 0.1 dex metallicity interval.

3. The stellar sample should be homogeneous in temperature and luminosity. We selected the F-G-K dwarfs and subgiants based on the literature data.

4. Binaries, variables, and stars with any chemical peculiarity (carbon-enhanced stars, low [α/Fe] stars, etc.) were excluded.

5. For testing purposes the stellar sample should include a dozen of well-studied stars of various metallicities, for which their stellar atmosphere parameters $T_{\rm eff}$ and log g were determined in the literature, presumably, from the non-spectroscopic methods.

Thus, 50 stars, in total, were selected, and they cover the $-2.6 <$ [Fe/H] $< +0.3$ metallicity range.

Spectra of 48 stars were obtained using the Hamilton Echelle Spectrograph mounted on the Shane 3-m telescope of the Lick observatory during the two observation runs March 15-16, 2011 and January 5-11, 2012. Most stars were observed, at least, twice. The resolving power is $R = \lambda/\Delta\lambda \simeq 60\,000$, and the spectral coverage is 3700 Å to 9300 Å. The signal-to-noise ratio (S/N) at 5500 Å is higher than 100 for most stars. The exception is BD -04° 3208, where $S/N(\lambda = 5500\text{Å}) \simeq 70$. It is worth noting that the spectra suffer from the fringing effect in the infrared band.

For two stars, we used the spectra observed with the ESPaDOnS echelle spectrograph at the 3.6-m telescope of the Canada-France-Hawaii (CFH) observatory in queued service observing mode during several nights in 2011 and 2012. The spectra cover 3700 Å to 10 450 Å. They have $R \simeq 81\,000$ and $S/N \simeq 150$ at 5030 Å and higher value of about 200 at 8090 Å.

The Shane/Hamilton spectra were reduced with the IRAF package following standard procedures that include the aperture definition, flat-field correction, background subtraction, one-dimensional spectra extraction, wavelength calibration, and continuum normalization. The wavelength calibration was performed using the lamp with the titanium cathode in argon environment. Such a lamp is rare in the astronomical observations, and an appropriate list of the Ti and Ar lines was compiled by Pakhomov & Zhao (2013). The uncertainty in wavelength calibration is estimated to be 0.006 Å.

The CFHT/ESPaDOnS spectra were reduced with the special reduction package Libre-ESpRIT[3], which includes two steps. The first one performs a geometrical analysis from a sequence of calibration exposures, and the second step achieves spectrum optimal extraction in itself, using the geometrical information derived in the first step. The reduction procedure returns the normalised spectra.

To improve the statistics of the VMP stars, we include the well-studied halo star HD 140283 in our sample. Its high-quality observed spectrum was taken from the ESO UVESPOP survey (Bagnulo et al. 2003). For seven stars our observational material was complemented with the data from different sources. We employed the

[3] http://www.cfht.hawaii.edu/Instruments/Spectroscopy/Espadons

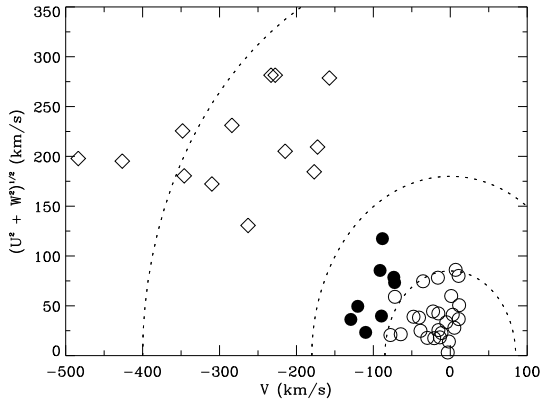

FIG. 1.— Toomre diagram for the investigated stars from the perspective of the local standard of rest. Dashed curves delineate constant peculiar space velocities $v_{pec} = (U^2+V^2+W^2)^{1/2} = 85$, 180, and 400 km s^{-1}. Different symbols show the thin disk (open circles), thick disk (filled circles), and halo (open rhombi) stars.

spectra obtained by Klaus Fuhrmann with the fiber optics Cassegrain echelle spectrograph FOCES at the 2.2-m telescope of the Calar Alto Observatory in 1996 to 2000 (Fuhrmann 1998, 2004). The star BD−04° 3208 was observed using UVES/VLT in April 2001 within our project 67.D-0086A (PI: T. Gehren). Details of spectra reduction were described by Mashonkina et al. (2003). For HD 49933 its high-quality spectrum was observed with the HARPS spectrograph at the 3.6-m ESO La Silla telescope. Details of spectra reduction were described by Ryabchikova et al. (2009).

This paper deals with 51 stars, in total. The investigated stars together with characteristics of the observed spectra are listed in Table 2.

3. KINEMATIC PROPERTIES OF THE SELECTED STARS

The stellar kinematics is closely related to stellar populations in the Galaxy, and it is commonly applied to identify a membership of given star to the galactic stellar populations, namely the thin disk, the thick disk, and the halo.

The galactic space velocity components U, V, W were calculated using the equations and formalism of Johnson & Soderblom (1987). They were defined with respect to the local standard of rest (LSR), adopting the standard solar motion (U, V, W) = (10.00, 5.25, 7.17) km s^{-1} of Dehnen & Binney (1998). In computations of the X, Y, Z-coordinates, we used the best current estimate of the Galactocentric distance of the Sun $R_G = 8.0$ kpc, which was inferred from a comparison of different statistical techniques (Malkin 2013). The parallaxes and proper motions were taken from the updated version of the HIPPARCOS catalogue (van Leeuwen 2007) and the radial velocities from the HIPPARCOS Input catalogue (Turon et al. 1993). The obtained results are presented in Table 3. The star BD −13° 3442 is missing in the HIPPARCOS catalogue, and it was assigned to the galactic halo based on its very low Fe abundance, with [Fe/H] = −2.62 (Sect. 5), and high proper motion as indicated by the Simbad database[4].

Following Fuhrmann (2000) and later studies (for example Chen et al. 2004; Bensby et al. 2010), we identify the stars with peculiar space velocities with respect to the LSR in the range 85 km s^{-1} < v_{pec} < 180 km s^{-1} as belonging to the thick disk stellar population, the stars with v_{pec} < 85 km s^{-1} to the thin disk, and all the halo stars of our sample have v_{pec} > 200 km s^{-1} (Fig. 1). The star G090-003 is not shown in Fig. 1, because its peculiar space velocity, $v_{pec} = 847 \pm 1580$ km s^{-1}, is rather uncertain due to large error of the HIPPARCOS parallax, $\pi = 1.12 \pm 2.14$ mas. For six stars with peculiar space velocities close to $v_{pec} = 85$ km s^{-1}, their membership to either the thin disk or the thick disk cannot be decided using only the kinematic properties. Following Fuhrmann (1998), we also took into account their chemical properties, as determined in Sect. 5. For example, HD 30562, with $v_{pec} = 93$ km s^{-1}, was assigned to the thin disk because it has a supersolar Fe abundance, with [Fe/H] = 0.17, and it does not reveal Mg enhancement relative to Fe.

4. METHOD OF CALCULATIONS

Stellar parameters of the selected sample were determined in this study applying different methods, including the spectroscopic one based on the NLTE analysis of lines of Fe I and Fe II. This section describes calculations of the theoretical spectra.

4.1. *Codes and model atmospheres*

The statistical equilibrium (SE) of Fe I-Fe II was calculated with a comprehensive model atom treated by Mashonkina et al. (2011). The main source of the uncertainty in the NLTE results for Fe I is poorly known inelastic collisions with hydrogen atoms. We employed the formula of Drawin (1968, 1969), as implemented by Steenbock & Holweger (1984), for allowed $b-b$ and $b-f$ transitions and a simple relation between hydrogen and electron collisional rates, $C_H = C_e\sqrt{(m_e/m_H)}N_H/N_e$, for forbidden transitions, following Takeda (1994). Mashonkina et al. (2011) recommended to scale the Drawin rates by a factor of $S_{\rm H}$ = 0.1 based on their analysis of element abundances derived from the two ionization stages, Fe I and Fe II, in the selected VMP stars. Bergemann et al. (2012) estimated a larger value of $S_{\rm H} = 1$. In this study, $S_{\rm H}$ was further constrained using the benchmark stars.

The coupled radiative transfer and SE equations were solved with a revised version of the DETAIL code (Butler & Giddings 1985). The update was presented by Mashonkina et al. (2011). The obtained departure coefficients were then used by the codes binmag3 (Kochukhov 2010), synthV-NLTE (Vadim Tsymbal, private communication, based on SynthV code Tsymbal 1996) and SIU (Reetz 1991) to calculate the synthetic line profiles.

We used the MARCS model structures (Gustafsson et al. 2008)[5], which were interpolated for given $T_{\rm eff}$, log g, and [Fe/H] using a FORTRAN-based routine written by Thomas Masseron[6].

4.2. *Selection of iron lines*

The investigated lines were selected according to the following criteria.

[4] http://simbad.u-strasbg.fr/simbad/

[5] http://marcs.astro.uu.se

[6] http://marcs.astro.uu.se/software.php

(i) The lines should be almost free of visible/known blends in the solar spectrum.

(ii) For Fe I the linelist should cover a range of excitation energies of the lower level, $E_{\rm exc}$, as large as possible to investigate the excitation equilibrium of neutral iron. On the other hand, the low-excitation ($E_{\rm exc} <$ 1.2 eV) lines in metal-poor stars often appear to have higher abundances than lines with higher excitation energy (see, for example Cayrel et al. 2004; Lai et al. 2008). The calculations with ab initio 3D, time-dependent, hydrodynamical model atmospheres of cool stars predict that the 3D effects for lines of Fe I are strongly $E_{\rm exc}$ dependent (Collet et al. 2007; Dobrovolskas et al. 2013). For example, the 3D abundance corrections amount to -0.8 dex and -0.25 dex for the $E_{\rm exc} = 0$ lines of Fe I in the models $T_{\rm eff}$ / log g / [M/H] = 5860/4/-2 and 5850/4/-1, respectively, while they are -0.2 dex and -0.07 dex for the $E_{\rm exc} = 2$ eV lines and close to 0 for the $E_{\rm exc} = 4$ eV lines (Dobrovolskas et al. 2013). To minimise a possible influence of the 3D effects on $T_{\rm eff}$ determinations, we did not consider lines of Fe I with $E_{\rm exc} < 2$ eV.

(iii) For both close-to-solar metallicity and VMP stars, lines of various strength have to be present in the spectrum to evaluate stellar microturbulence velocity ξ_t.

For individual stars, we also avoided using of saturated lines with the equivalent width $EW > 180$ mÅ to minimise an influence of possible uncertainty in the van der Waals damping constants on final abundances.

The selected lines are listed in Table 4 along with their atomic parameters. For neutral iron we employed experimental gf-values from Blackwell et al. (1979, 1982a,b); O'Brian et al. (1991), and Bard et al. (1991). Two sets of oscillator strengths from Meléndez & Barbuy (2009) and Raassen & Uylings (1998) were inspected for Fe II. Van der Waals broadening of the selected lines is accounted for using the most accurate data as provided by Barklem et al. (2000) for Fe I and Barklem & Aspelund-Johansson (2005) for Fe II.

4.3. *Sun as a reference star*

To minimise the effect of the uncertainty in gf-values on the final results, we applied a line-by-line differential NLTE and LTE approach, in the sense that stellar line abundances were compared with individual abundances of their solar counterparts. The solar flux observations were taken from the Kitt Peak Solar Flux Atlas (Kurucz et al. 1984). The calculations were performed with the MARCS model atmosphere 5777/4.44/0. A microturbulence velocity of 0.9 km s^{-1} was adopted.

The solar LTE and NLTE abundances from individual lines are presented in Table 4. The NLTE calculatoins were performed using $S_{\rm H} = 0.5$ (see sect. 5). For the Fe I lines, the solar mean LTE and NLTE abundances are $\log A_{\rm LTE} = -4.57 \pm 0.09$ and $\log A_{\rm NLTE} = -4.56 \pm 0.09$. Hereafter, $A_X = N_X/N_{tot}$ is the element abundance taken relative to the total number of atoms. For lines of Fe II, the NLTE abundance corrections do not exceed 0.01 dex, in absolute value, and the solar mean abundance amounts to $\log A = -4.56 \pm 0.05$ and $\log A = -4.50 \pm 0.05$, when using gf-values from Meléndez & Barbuy (2009) and Raassen & Uylings (1998), respectively. Hereafter, the statistical abundance error is the dispersion in the single line measurements about the mean: $\sigma = \sqrt{\Sigma(x - x_i)^2/(N-1)}$, where N is the total number of lines used, x is their mean abundance, x_i the individual abundance of each line. It is worth noting that an uncertainty of 0.06 dex in abundance from the Fe II lines leads to an 0.12 dex uncertainty in log g for solar-type stars. This is crucial for surface gravity determinations from the Fe I/Fe II ionization equilibrium.

5. DETERMINATION OF STELLAR PARAMETERS

To derive atmospheric parameters of our stellar sample, the following strategy was applied. First, we selected the stars, for which their effective temperatures and surface gravities were determined reliably using the non-spectroscopic methods, namely $T_{\rm eff}$ from the infrared flux method (IRFM) and log g from the well-known relation between log g, stellar mass M, $T_{\rm eff}$, and absolute bolometric magnitude $M_{\rm bol}$:

$$[g] = [M] + 4[T_{\rm eff}] + 0.4(M_{\rm bol} - M_{\rm bol\odot}). \quad (1)$$

Here, square brackets denote the logarithmic ratio with respect to the solar value. The $M_{\rm bol}$ magnitudes were obtained using the V magnitudes from Olsen (1983, 1993), the revised Hipparcos parallaxes of van Leeuwen (2007), and the bolometric corrections (BC) from Alonso et al. (1995). For the Sun the absolute visual magnitude $M_{V\odot} = 4.87$ and $BC_\odot = -0.12$ were adopted. The star's mass was estimated from its position in the $M_{\rm bol}$ - $\log T_{\rm eff}$ diagram by interpolating in the Dartmouth isochrones (Dotter et al. 2008). "Reliably" means that multiple measurements of the IRFM temperature are available and the uncertainty in the Hipparcos parallax based surface gravity, log g_{Hip}, is less than 0.1 dex. This implies a parallax error of smaller than 10 %. The 20 stars in our sample meet these requirements. They are listed in Table 5 as the benchmark stars.

Atmospheric parameters of the remaining stars were derived or improved spectroscopically from the NLTE analysis of lines of Fe I and Fe II.

In the stellar parameter range, with which we concern, lines of Fe I are weakened towards higher $T_{\rm eff}$, resulting in higher derived element abundance, while they are nearly insensitive to variation in log g. In contrast, lines of Fe II are only weakly sensitive to variation in $T_{\rm eff}$, while they are weakened with log g increasing. If $T_{\rm eff}$ is fixed, the surface gravity is obtained from the requirement that abundances from lines of Fe I and Fe II must be equal. One needs to be cautious, when deriving both $T_{\rm eff}$ and log g from Fe I and Fe II. Any shift in $T_{\rm eff}$ leads to shifting log g in the sense: an increase in $T_{\rm eff}$ leads to an increase in log g. Therefore, in this study we used non-spectroscopic (IRFM) determinations of $T_{\rm eff}$, where available, and for every star its final parameters, $T_{\rm eff}$/log g/[Fe/H], were checked with the corresponding evolutionary track.

For each benchmark star, abundances from lines of Fe I and Fe II were derived under various line-formation assumptions, i.e., NLTE with $S_{\rm H} = 0.1$, 0.5, 1 and LTE, and we investigated which of them leads to consistent element abundances from both ionization stages. Our calculations showed that the departures from LTE are small for the [Fe/H] > -1 stars. Indeed, in this metallicity range the NLTE abundance correction, $\Delta_{\rm NLTE} =$

TABLE 1
ABUNDANCE DIFFERENCES FE I - FE II IN THE SELECTED THREE STARS FOR DIFFERENT LINE FORMATION SCENARIOS.

HD	LTE	NLTE		
		$S_{\rm H}$ = 1	$S_{\rm H}$ = 0.5	$S_{\rm H}$ = 0.1
84937	-0.06	-0.02	0.00	0.11
94028	-0.06	-0.05	-0.04	-0.01
140283	-0.06	-0.04	-0.02	0.10

$\log A_{\rm NLTE} - \log A_{\rm LTE}$, does not exceed 0.04 dex for $S_{\rm H}$ = 0.5, and the difference in NLTE abundances between $S_{\rm H}$ = 0.1 and 0.5 is smaller than 0.04 dex. The three of six [Fe/H] < -1 stars are cool, with $T_{\rm eff} \leq 5400$ K, and they are not useful for constraining $S_{\rm H}$ because of small $\Delta_{\rm NLTE} \leq 0.02$ dex. Table 1 lists the abundance differences between Fe I and Fe II from the calculations with different $S_{\rm H}$ for the three benchmark stars with the largest NLTE effects. For every star, the acceptable abundance difference is achieved with $S_{\rm H}$ = 0.5 and 1. Hereafter, we choose $S_{\rm H}$ = 0.5 to perform the NLTE calculations for Fe I-FeII.

Spectroscopic stellar parameters were obtained in the iterative procedure. For each star, our initial guess was $T_{\rm eff} = T_{\rm IRFM}$, if available, or $T_{\rm eff} = T_{b-y}$ and log g = log g_{Hip}. Effective temperature and surface gravity were corrected until the ionisation equilibrium between Fe I and Fe II and the Fe I excitation equilibrium were fulfilled.

5.1. *Effective temperatures*

Although there are multiple measurements of the IRFM effective temperature for individual stars of our sample (Alonso et al. 1996a; González Hernández & Bonifacio 2009; Casagrande et al. 2010, 2011), we found no study that provides the data for every investigated star. Figure 2 (top panel) displays the differences between different sources for the stars in common with this work. It can be seen that the $T_{\rm eff}$ scale of Casagrande et al. (2011, C11) is hotter than that of Alonso et al. (1996a, A96), with $\Delta T_{\rm IRFM}$(C11 - A96) = 114 ± 62 K for 25 stars. The difference between C11 and González Hernández & Bonifacio (2009, GB09) is smaller, $\Delta T_{\rm IRFM}$(C11 - GB09) = 32 ± 83 K for 26 stars. Here, we did not count the two outliers HD 34411 and HD 142373, with large uncertainties in $T_{\rm IRFM}$ of 479 K and 342 K, respectively, that were caused by using saturated 2MASS photometry.

We calculated four sets of the photometric temperatures from the $b-y$ and $V-K$ colour indices using two different calibrations of Casagrande et al. (2010, C10) and Alonso et al. (1996b). The V magnitudes and $b-y$ colours were taken from Olsen (1983, 1993) for 45 stars, in total, and the K magnitudes from the 2MASS catalogue (Skrutskie et al. 2006) for 24 stars, in total. Figure 2 display the differences between $T_{\rm IRFM}$ and T_{b-y} for both effective temperature scales. We found that T_{b-y} and T_{V-K} agree well with those from the IRFM, when using the calibrations of C10, with $T_{\rm IRFM}$(C11) – T_{b-y}(C10) = 10 ± 46 K (42 stars) and $T_{\rm IRFM}$(C11) – T_{V-K}(C10) = 22 ± 68 K (21 stars). For the Alonso et al. (1996b) calibration, the differences are

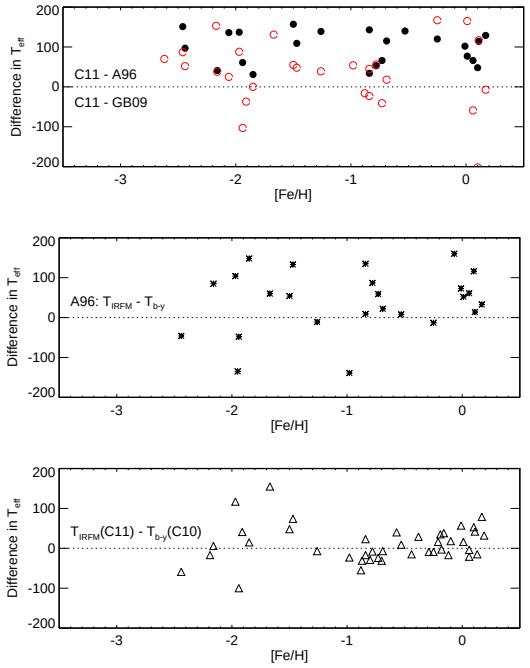

FIG. 2.— Top panel: differences in the IRFM effective temperatures of the investigated stars between Casagrande et al. (2011, C11) and Alonso et al. (1996a, A96) (filled circles) and between C11 and González Hernández & Bonifacio (2009, GB09) (open circles). Middle panel: differences $T_{\rm IRFM}$(A96) – T_{b-y}(Alonso et al. 1996b). Bottom panel: differences $T_{\rm IRFM}$(C11) – T_{b-y}(Casagrande et al. 2010, C10).

larger, with $T_{\rm IRFM}$(A96) – T_{b-y} = 41 ± 78 K (25 stars) and $T_{\rm IRFM}$(A96) – T_{V-K} = 72 ± 58 K (12 stars), although the statistics is small for the $V-K$ photometry.

For the *benchmark stars*, we aimed to have a homogeneous set of $T_{\rm eff}$ based on a single source of the IRFM temperatures. The only study that provides $T_{\rm IRFM}$ for every benchmark star is GB09. Using their $T_{\rm IRFM}$, we could not achieve the Fe I/Fe II ionization equilibrium and the Fe I excitation equilibrium for half benchmark stars, independent of applying either LTE or NLTE approach. No preference was, therefore, given to any source of $T_{\rm IRFM}$. Instead, for each star its temperature from A96, GB09, C10, and C11, where available, and the corresponding log g_{Hip} value were checked with the difference in NLTE abundances between Fe I and Fe II and a slope of the [Fe/H] versus $E_{\rm exc}$ plot for Fe I. For six stars, corrections up to 50 K were applied to the most appropiate $T_{\rm IRFM}$ to obtain the final effective temperature (Table 5).

5.2. *Surface gravities, metallicities, and microturbulence velocities*

For each benchmark star, the NLTE abundances from the two ionization stages, Fe I and Fe II, were found to be consistent within 0.06 dex. Hereafter, 0.06 dex was considered as an admissible difference between Fe I and Fe II, when deriving spectroscopic stellar parameters of the remaining, non-benchmark, stars. For given star, we started from checking the photometric temperature, $T_{\rm IRFM}$ or T_{b-y}, and the HIPPARCOS parallax based gravity, log g_{Hip}. Effective temperature and surface gravity were allowed to vary within the corresponding error bars. The procedure was iterated until the NLTE abundance

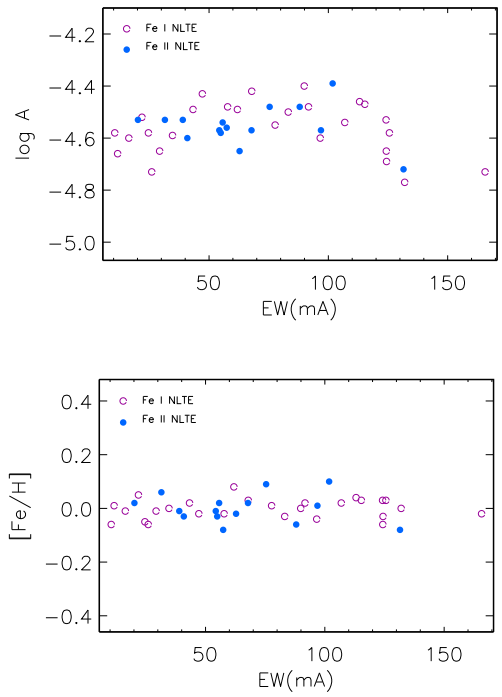

FIG. 3.— Absolute (top panel) and differential (bottom panel) NLTE abundances from lines of Fe I (open circles) and Fe II (filled circles) in HD 22484.

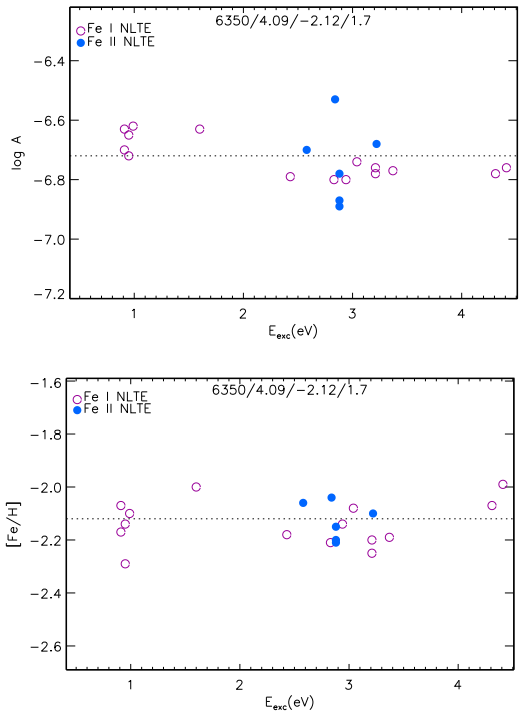

FIG. 4.— Absolute (top panel) and differential (bottom panel) NLTE abundances from lines of Fe I (open circles) and Fe II (filled circles) in HD 84937.

difference Fe I – Fe II is getting smaller than 0.06 dex, the excitation trend for Fe I disappears, and lines of different equivalent width give consistent iron abundances.

We found that the differential approach largely removes a line-to-line scatter for the [Fe/H] ≥ -1.5 stars. For example, when moving from the absolute to the differential NLTE abundances, the dispersion reduces from $\sigma = 0.10$ dex to $\sigma = 0.04$ dex for lines of Fe I and from $\sigma = 0.08$ dex to $\sigma = 0.05$ dex for lines of Fe II in HD 22484 (6000/4.07/0.01, Fig. 3). For more metal-poor stars, the differential approach is less efficient in removing a line-to-line scatter. For example, for HD 84937 (6350/4.09/−2.12) the scatter of data reduces for Fe II, but not Fe I lines (Fig. 4). When using the $E_{\rm exc} > 2$ eV lines of Fe I, we obtained $\sigma = 0.035$ dex and 0.078 dex for the absolute and differential abundances, respectively. This is, probably, due to the uncertainties in the van der Waals damping constant, C_6. The lines, which can be measured in the VMP stars, have strong van der Waals broadened wings in the solar spectrum (for example Fe I 5383 Å, Fig. 5). For such a line, the uncertainty in the derived solar abundance is contributed from the uncertainties in both gf- and C_6-values. When dealing with the VMP stars, the differential analysis is able to cancel the uncertainty in gf, but not C_6.

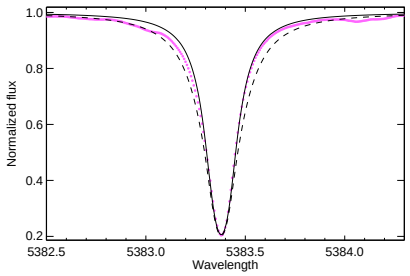

FIG. 5.— Theoretical NLTE profiles of Fe I 5383 Å computed with $\log C_6 = -30.370$ (Barklem et al. 2000, dashed curve) and $\log C_6 = -31.095$ Kurucz (2007, continuous curve) compared to the solar spectrum (Kurucz et al. 1984, bold dots). Everywhere in the calculations, $\log A_{\rm Fe} = -4.54$. To fit the solar line profile with $\log C_6 = -30.370$, one needs to reduce the iron abundance down to $\log A_{\rm Fe} = -4.72$.

Although our final results are based on using the $E_{\rm exc} \geq 2$ eV lines of Fe I, for most stars we also checked abundances determined from the lower excitation lines. We found no abundance difference between the low and high excitation lines for close-to-solar metallicity stars. For the most metal-poor stars, such as HD 84937, the absolute abundances reveal an excitation trend, but it disappears for the differential abundances (Fig. 4).

We did not determine stellar parameters under the LTE assumption and cannot evaluate the differences in log g between using LTE and NLTE. However, the NLTE effects can be estimated based on our LTE and NLTE calculations for Fe I-Fe II and the sensitivity of iron lines to variation in log g. Since the departures from LTE lead to weakened lines of Fe I, but they do not affect lines of Fe II until the extremely low metallicities, the ionization equilibrium Fe I/Fe II is achieved for higher gravities in NLTE than in LTE. The shifts in log g increase towards lower metallicity and surface gravity. For our program stars they may be up to 0.1 dex at [Fe/H] > -1.5, up to 0.2 dex for $-2.2 <$ [Fe/H] < -1.8 and reach 0.45 dex for the most MP star of our sample BD -13° 3442, with [Fe/H] $= -2.62$.

5.3. *Checking atmospheric parameters with evolutionary tracks*

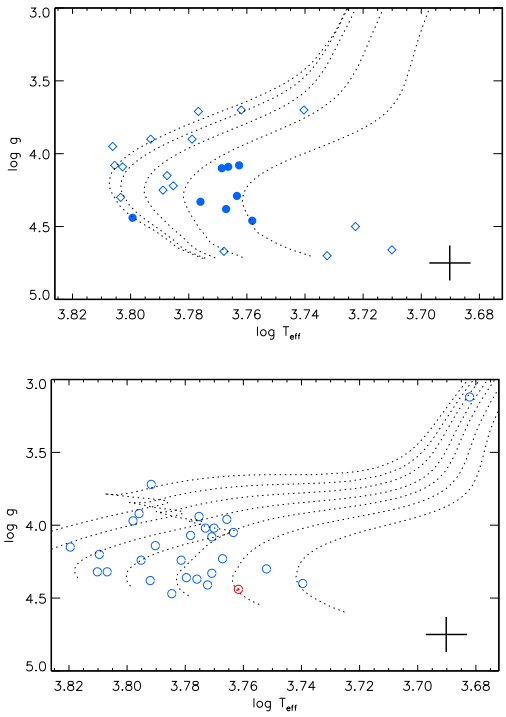

FIG. 6.— Top panel: investigated thick disc (filled circles) and halo (diamonds) stars compared with the evolutionary tracks of M = 0.75 $M_{\odot}$ and [Fe/H] from −2.75 to −0.75 (from left to right), with a step of 0.5 dex. Bottom panel: the thin disc stars (open circles) compared with the evolutionary tracks of the solar metallicity and the stellar mass varying between $M = 0.9\,M_{\odot}$ and $1.5\,M_{\odot}$, with a step of $0.1M_{\odot}$. The crosses in each panel indicate log g and $T_{\rm eff}$ error bars of 0.12 dex and 80 K, respectively.

For each star the obtained effective temperature and surface gravity were checked by comparing its position in the log g – $T_{\rm eff}$ plane with the theoretical evolutionary track of given metallicity and α-enhancement in the Yi et al. (2004) grid (Fig. 6). An α-enhancement was assumed to be equal to [Mg/Fe] as derived in this study and presented in Table 3. Stellar masses corresponding to the best fit evolutionary tracks are indicated in Table 5. They range between 0.60 and 0.85 solar mass for the halo and thick disk stars that does not contradict with their evolutionary status and old age. For the thin disk stars, their masses range between 0.85 $M_{\odot}$ and 1.5 $M_{\odot}$ and ages between 1 Gyr and 9 Gyr.

For two halo cool dwarfs we had to revise $T_{\rm eff}$ / log g, to enforce the stars to sit on the main sequence of the appropriate evolutionary track. We stress that the changes in atmospheric parameters were not allowed to destroy the ionization equilibrium between Fe I and Fe II and the Fe I excitation equilibrium. For HD 64090, we adopted $T_{\rm eff}$ = 5400 K, which is close to $T_{\rm IRFM}$ = 5440 K (A96), and log g = 4.70, which is $1.5\sigma_{\rm logg}$ higher than log g_{Hip}. For BD +66°0268 our final temperature, $T_{\rm eff}$ = 5300 K, is close to $T_{\rm IRFM}$ = 5280 K (A96) and log g = 4.72 is $2\sigma_{\rm logg}$ higher than log g_{Hip}.

5.4. *Final atmospheric parameters*

The final atmospheric parameters together with the NLTE and LTE abundance differences between Fe I and Fe II are presented in Table 5. For the star's metallicity we adopted [Fe/H] determined from lines of Fe II, although the difference in NLTE abundances between Fe I and Fe II nowhere exceeds 0.06 dex. The Fe I – Fe II abundance differences are also shown in Fig. 7. In NLTE, they reveal no trends with any atmospheric parameter, either [Fe/H], or $T_{\rm eff}$, or log g.

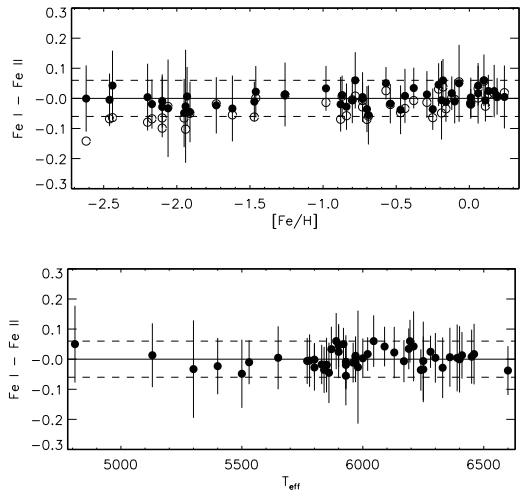

FIG. 7.— NLTE (filled circles) and LTE (open circles, top panel only) abundance differences Fe I – Fe II for the investigated stars. Dashed lines indicate an admissible difference of ±0.06 dex.

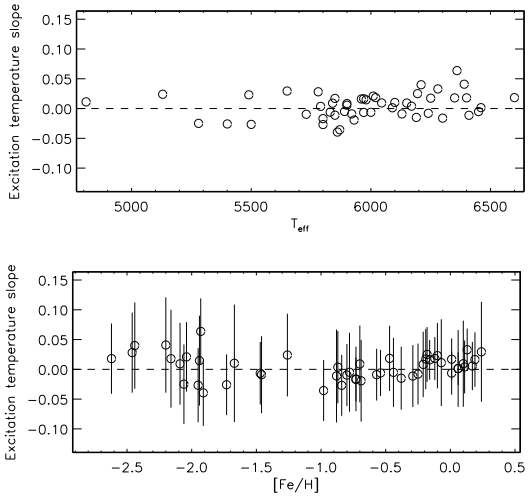

FIG. 8.— Excitation temperature slopes from Fe I lines for the investigated stars.

Figure 8 displays the excitation temperature slopes, d[Fe/H]/d$E_{\rm exc}$, calculated from lines of Fe I in the individual stars. The data reveal no trend with effective temperature, and d[Fe/H]/$dE_{\rm exc}$ = 0.0044 dex/eV, on average. The excitation slope seems to depend slightly on metallicity at [Fe/H] ≥ −1, although nowhere its magnitude exceeds the error bars. The scatter of data is larger for the [Fe/H] < −1.8 than less metal-poor stars due to smaller number of observed lines of Fe I.

In Fig. 9 we compare surface gravities from the Fe I/Fe II NLTE ionization equilibrium and Hipparcos parallax methods for the 20 stars, which do not belong to the benchmark stellar sample, but have a relative parallax uncertainty less than 10 %. The differences are minor, with Δlog g(Sp – Hip) = 0.008 ± 0.037 dex, on average, and they do not show any trends with surface gravity or effective temperature. Having in mind that

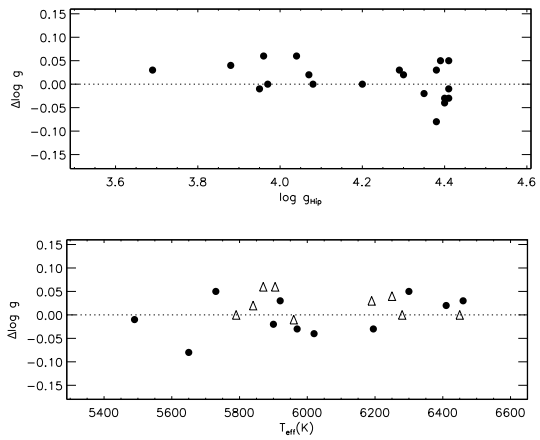

FIG. 9.— Differences in surface gravity from the Fe I/Fe II NLTE ionization equilibrium and Hipparcos parallax methods for 20 stars with the spectroscopically derived atmospheric parameters and a relative parallax uncertainty less than 10 %. In the bottom panel, the filled circles and open triangles show stars with log $g_{Hip} > 4.2$ and ≤ 4.2, respectively.

for each benchmark star the Fe I/Fe II ionization equilibrium was achieved with log g from the Hipparcos parallax method, we infer that the spectroscopic method of gravity determination is working in the 5130 K $\leq T_{\rm eff} \leq$ 6600 K and 3.12 $\leq$ log g $\leq$ 4.66 range. An exception is HD 64090, for which we determined log $g_{Sp} = 4.70$ that is 0.13 dex higher than log g_{Hip}. We, thus, do not confirm a temperature trend of Δlog g(Sp – Hip) for cool ($T_{\rm eff} < 5300$ K) dwarf (log g > 4.2) stars obtained by Bensby et al. (2014).

Final slopes of the [Fe/H] vs. *EW* plots amount to -0.0002 dex/mÅ, on average. Using the derived microturbulence velocities ξ_t and basic atmosheric parameters $T_{\rm eff}$, log g, and [Fe/H], we built up the approximation formula:

$$\xi_t = -0.21 + 0.06 \times [\mathrm{Fe/H}] + 5.6 \times (T_{\rm eff}/10^4) - 0.43 \times \log g. \quad (2)$$

Microturbulence velocity grows towards higher $T_{\rm eff}$ and lower surface gravity. The metallicity dependence is weak. Similar relations were previously found by other authors, for example Nissen (1981); Edvardsson et al. (1993); Allende Prieto et al. (2004), and Ramírez et al. (2013). In the first three studies theirs formulae did not include the [Fe/H] term because these studies dealt with the limited metallicity range. Using the formula (2) results in $\xi_t = 1.1\,\mathrm{km\,s^{-1}}$ and $1.4\,\mathrm{km\,s^{-1}}$ for the solar atmospheric parameters and 6000/4.0/−1.0, respectively. For comparison, the corresponding values are $1.1\,\mathrm{km\,s^{-1}}$ and $1.5\,\mathrm{km\,s^{-1}}$ from the Ramírez et al. (2013) formula.

5.5. *Notes on individual stars*

We provide additional comments on stars that turned out to be interesting for one or the other reason in the course of the analysis.

HD 59984 and HD 105755, with [Fe/H] = −0.69 and −0.73, respectively, may be the most metal-poor thin-disk stars. Both kinematics, $v_{pec} = 25\,\mathrm{km\,s^{-1}}$ and $28\,\mathrm{km\,s^{-1}}$, and an age of 8 Gyr for both stars support their thin-disk status.

HD 106516: We failed to obtain self-consistent stellar parameters for this star. On the one hand, the star exhibits a typical thick-disk kinematics, $v_{pec} = 108\,\mathrm{km\,s^{-1}}$, and chemical signatures, [Mg/Fe] = 0.38 and [Fe/H] = −0.73. On the other hand, its age was estimated to be 6 Gyr and unlikely older than 9 Gyr, identifying the star as a thin-disk star. According to Carney et al. (2001), it is a single-lined spectroscopic binary, with the period P = 843.9 days.

HD 134169: kinematics, $v_{pec} = 5\,\mathrm{km\,s^{-1}}$ identifies it as a thin-disk star. However, HD 134169 exhibits a typical thick-disk chemical signatures, [Mg/Fe] = 0.32 and [Fe/H] = −0.78, and old age, $\tau \simeq 11$ Gyr. Enhancement of Al relative to Fe, with [Al/Fe] = 0.54, found by Gehren et al. (2006) also suggests a thick-disk origin.

BD +37° 1458: this is a halo star. With spectroscopic $T_{\rm eff}$ = 5500 K, log g = 3.70, and [Fe/H] = −1.95, the star sits on the evolutionary track of $M = 0.67 M_{\odot}$ at τ = 24 Gyr. The younger age can only be obtained for higher $T_{\rm eff}$ and log g. However, there is no ground for a substantial revision of atmospheric parameters. The star's temperature is well fixed by several studies. Alonso et al. (1996a); Ramírez & Meléndez (2005), and González Hernández & Bonifacio (2009) derived $T_{\rm IRFM}$ = 5510 K, 5516 K, and 5582 K, respectively. Axer et al. (1994) determined $T_{\rm eff}$ = 5450 K from the Balmer line wing fits. With $T_{\rm eff}$ = 5500 K, log $g_{Hip} = 3.41 \pm 0.18$ is even lower than the spectroscopically derived value. For this star we choose the spectroscopic stellar parameters as the final ones.

5.6. *Uncertainties in derived atmospheric parameters*

The following approaches were applied to evaluate the uncertainties in the derived atmospheric parameters.

For the benchmark stars we adopted the $T_{\rm IRFM}$ errors as indicated by the original sources. Statistical error of the Hipparcos parallax based surface gravity was computed as the quadratic sum of errors of the star's parallax, effective temperature, mass, visual magnitude, and bolometric correction:

$$\sigma^2_{\rm logg} = (2\sigma_{\log \pi})^2 + (4\sigma_{\log T})^2 + \sigma^2_{\log M} + (0.4\sigma_V)^2 + (0.4\sigma_{\rm BC})^2.$$

The uncertainties in V magnitude and bolometric correction together contribute less than 0.01 dex to the total log g error. For $T_{\rm eff}$ the contribution nowhere exceeds 0.03 dex. Stellar masses were well constrained using the evolutionary tracks, with an uncertainty of no more than 0.1 $M_{\odot}$, resulting in 0.04 dex contribution to $\sigma_{\rm logg}$.

In Fig. 10 our final $T_{\rm eff}$s are compared with the IRFM temperatures from C11 and A96. For 47 stars in common with C11, our values are 51 K, on average, lower. In contrast, this study determined 46 K higher temperatures compared with that of A96 for 29 common stars. We note very similar statistical errors of 63 K and 69 K for the temperature differences (this work – C11) and (this work – A96), respectively. Based on these comparisons, we estimate the systematic and statistical errors of $T_{\rm eff}$ for the 31 stars with the spectroscopically derived atmospheric parameters to be 50 K and 70 K.

For 20 stars with the spectroscopic surface gravities, log g_{Sp}, their HIPPARCOS parallaxes were measured with a relative parallax error less than 10 %, and we calculated reliable log g_{Hip} values. As shown in Fig. 9, log g_{Sp} – log $g_{Hip} = 0.008 \pm 0.037$ dex. This led us to estimate the uncertainty in log g_{Sp} to be 0.04 dex.

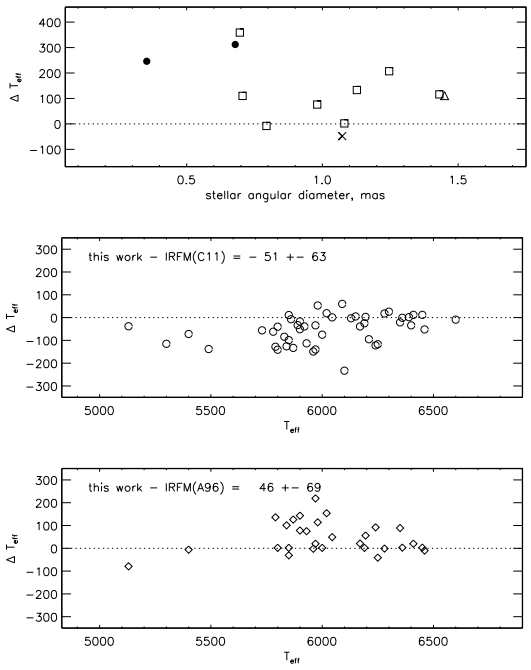

FIG. 10.— Differences in effective temperature between this study and the literature data. The top panel corresponds to interferometric measurements of Boyajian et al. (2012, 2013, squares), Creevey et al. (2012, 2015, filled circles), North et al. (2009, triangle), and von Braun et al. (2014, cross). See sect. 6 for more details. The middle and bottom panels use the IRFM temperatures from Casagrande et al. (2011) and Alonso et al. (1996b), respectively.

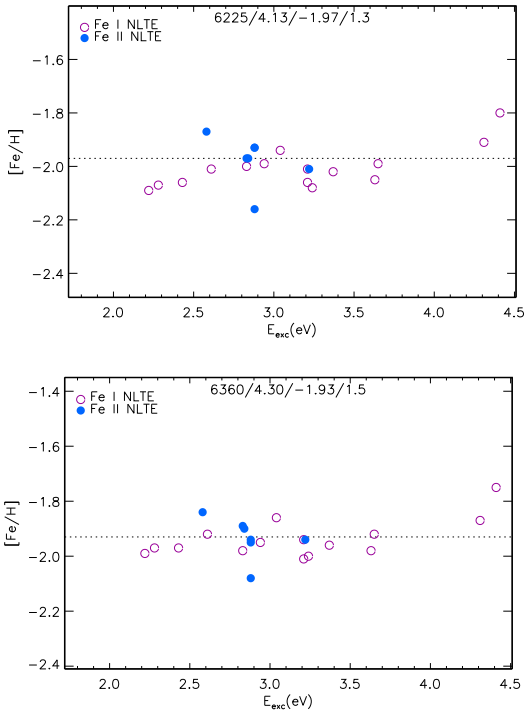

FIG. 11.— Impact of changes in $T_{\rm eff}$ and log g on the NLTE differential abundances derived from the Fe I (open circles) and Fe II (filled circles) lines in HD 74000. The top panel corresponds to our final parameters, $T_{\rm eff}$ = 6225 K, log g = 4.13, [Fe/H] = −1.97, and the bottom one to $T_{\rm eff}$ = 6360 K, log g = 4.30, [Fe/H] = −1.93. The differences in NLTE abundances Fe I – Fe II = −0.03 dex and +0.01 dex, respectively.

Statistical error of [Fe/H] was defined by the dispersion, σ, for lines of Fe II in given star.

Statistical error of the microturbulence velocity was adopted to be common for the whole stellar sample, and it was defined by the dispersion in the single ξ_t measurements about the relation (2). It amounts to 0.14 km s^{-1}.

It is worth noting that the uncertainty in spectroscopically derived atmospheric parameters can be larger than that quoted above. For example, for the halo star HD 74000 we found the two sets of stellar parameters that reproduce well the Fe I/Fe II ionization and Fe I excitaion equilibrium (Fig. 11) and fit the appropriate evolutionary tracks. These are $T_{\rm eff}$ = 6225 K, log g = 4.13, and [Fe/H] = −1.97 suggesting the star's age of 15 Gyr and $T_{\rm eff}$ = 6360 K, log g = 4.30, and [Fe/H] = −1.93 resulting in τ = 13.5 Gyr. The first set relied, in fact, on $T_{\rm IRFM}$(A96) and the second one on $T_{\rm IRFM}$(C11). A shift of +135 K in $T_{\rm eff}$ leads to +0.17 dex shift in log g, and both sets of parameters provide an acceptable star's age. No of two sets can be preferred from a comparison of log g_{Sp} with the corresponding HIPPARCOS parallax based surface gravity, log g_{Hip} = 4.16 ± 0.16 for $T_{\rm eff}$ = 6225 K and log g_{Hip} = 4.20 ± 0.16 for $T_{\rm eff}$ = 6360 K. From analysis of H_α and H_β in HD 74000 Mashonkina et al. (2003) inferred $T_{\rm eff}$ = 6225 K. Two pairs of $T_{\rm eff}$ / log g, which provide the Fe I/Fe II ionization equilibrium and reasonable star's mass and age, were also obtained for HD 108177 (6100/4.22/−1.67 and 6250/4.40/−1.62), and G090-003 (6100/3.90/−2.04 and 5930/3.80/−2.10). We, therefore, recommend to apply various spectroscopic and non-spectroscopic methods to given star to find an unique solution for the star's $T_{\rm eff}$ / log g.

6. COMPARISON WITH OTHER STUDIES

For ten stars of our sample, their $T_{\rm eff}$s were determined in the literature based on measurements of the angular diameters, trigonometric parallaxes, and bolometric fluxes. Boyajian et al. (2013, B13) published the most numerous list of the interferometric temperatures, T_{int}, based on angular diameters measured with the CHARA array (330 m maximum baseline). Figure 10 displays the temperature differences between this study and interferometric measurements of B13, North et al. (2009); Creevey et al. (2012, 2015), and von Braun et al. (2014). Our values are, on average, higher, with $\Delta T_{\rm eff}$ = 135 ± 126 K for ten stars and 78 ± 81 K, when excluding the two outliers, HD 103095 and HD 140283. We selected three stars for a detailed comparison.

HD 102870. Two successive determinations of Boyajian et al. (2012) and B13 resulted in T_{int} = 6132 K and 6054 K, with small temperature errors of 36 K and 13 K, respectively. A downward revision by 78 K was due to employing the different bolometric fluxes. The most recent temperature of B13 is in line with the earlier data of North et al. (2009), T_{int} = 6059 ± 49 K. Surface gravity based on the asteroseismic measurements amounts to log g_{seis} = 4.11 ± 0.02 (Creevey et al. 2013). With $T_{\rm eff}$ = 6060 K and log g = 4.11, we failed to achieve the ionization equilibrium between Fe I and Fe II and obtained Fe I – Fe II = −0.12 dex in NLTE. It is worth noting, log g_{Hip} = 4.14 adopted in this study agrees well with log g_{seis}. For solar-type stars the asteroseismology method depends only weakly on $T_{\rm eff}$. Indeed, a 200 K

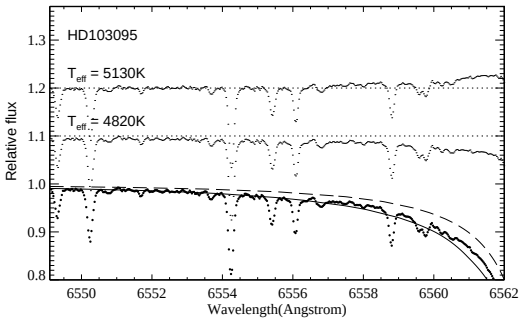

FIG. 12.— Theoretical NLTE flux profiles of H_α calculated with $T_{\rm eff}$ = 4820 K (dashed curve) and $T_{\rm eff}$ = 5130 K (continuous curve) compared to the observed FOCES spectrum of HD 103095 (bold dots). The differences between observed and calculated spectra, (O - C), are shown in the upper part of the panel.

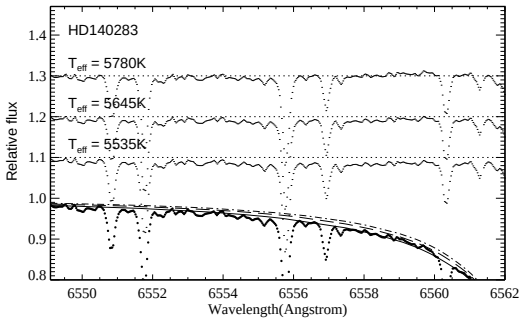

FIG. 13.— Theoretical NLTE flux profiles of H_α calculated with $T_{\rm eff}$ = 5535 K (dash-dotted curve), 5645 K (dashed curve), and 5780 K (continuous curve) compared to the observed VLT/UVES spectrum of HD 140283 (bold dots). The (O - C) values are shown in the upper part of the panel.

temperature difference produces a difference of 0.007 dex in log g. To obtain consistent NLTE abundances from lines of Fe I and Fe II using log g = 4.14, one needs to have 110 K higher temperature of HD 102870 (Table 5) compared with its T_{int}.

HD 103095. Using the CHARA array measurements, B13 and Creevey et al. (2012) derived T_{int} = 4771 ± 18 K and 4818 ± 54 K, respectively. We checked $T_{\rm eff}$ = 4820 K and log g_{Hip} = 4.60 with various spectroscopic temperature and gravity indicators.

(i) The Fe I/Fe II ionization equilibrium is not fulfilled, and the NLTE abundance difference amounts to Fe I – Fe II = −0.27 dex.

(ii) We compared the NLTE abundances from C I 9094 Å, 9111 Å with the carbon abundance from a number of molecular CH bands, which are known to be sensitive to $T_{\rm eff}$ variation. The NLTE method for C I and atomic and molecular data were taken from Alexeeva & Mashonkina (2015). With the 4820/4.60/−1.3 model, the abundance difference, C I – CH = 0.56 dex, is very large, while it amounts to −0.06 dex for our final parameters, $T_{\rm eff}$ = 5130 K and log g = 4.66.

(iii) Effective temperature can also be constrained from analysis of the H_α line wings (Fig. 12). The theoretical NLTE profiles of H_α were computed following Mashonkina et al. (2008). It can be seen that $T_{\rm eff}$ = 4820 K leads to shallower wings of H_α compared with the observations, but $T_{\rm eff}$ = 5130 K to deeper core-to-wing transition region. The best fit was achieved for $T_{\rm eff}$ = 5030 K. It is worth noting, Cayrel et al. (2011) obtained 100 K, on average, lower temperatures from the H_α line wings compared with accurate effective temperatures from the apparent angular diameter for the eleven FGK-type stars in the $-0.7 \le$ [Fe/H] ≤ 0.2 range. In contrast, T_{int} = 4771 K and 4818 K of HD 103095, as determined by B13 and Creevey et al. (2012), respectively, are more than 200 K lower than the temperature from H_α.

Thus, no spectroscopic temperature indicator supports the literature data on T_{int} for HD 103095.

HD 140283. Creevey et al. (2015) derived T_{int} = 5534 ± 103 K and 5647 ± 105 K assuming zero-reddening and $A_V = 0.1^m$, respectively. It is worth noting, HD 140283 is a nearby star, at a distance of 58 pc from the Sun, and an interstellar absorption of $A_V = 0.1^m$ is unlikely produced. Of the two temperatures T_{int} = 5534 K should be preferred, nevertheless we checked both using the same spectroscopic indicators as for HD 103095. The NLTE abundance differences Fe I – Fe II were found to be −0.18 dex and −0.09 dex, respectively. For both temperatures an abundance difference between carbon atomic and molecular lines is large, with (C I – CH) = 0.69 dex and 0.32 dex, while consistent abundances, (C I – CH) = 0.00 dex, were obtained for our final parameters, $T_{\rm eff}$ = 5780 K and log g = 3.70. Figure 13 shows theoretical profiles of H_α in the three different model atmospheres compared with the observed spectrum of HD 140283. It is evident that T_{int} = 5534 K is too low and it does not fit any spectroscopic indicator of $T_{\rm eff}$.

It is worth noting, both HD 103095 and HD 140283 have rather small angular diameters, θ_{int} = 0.679 ± 0.007 mas (Creevey et al. 2012) and 0.353 ± 0.013 mas (Creevey et al. 2015), respectively, which can be overestimated resulting in underestimated temperatures. Indeed, Casagrande et al. (2014) suspected systematic trends in the Boyajian et al. (2012, B12) dataset that was also based on the CHARA array interferometric measurements. They obtained the differences ($T_{\rm IRFM}$(C11) - T_{int}(B12)) growing towards smaller angular diameter and reaching +200 K, on average, at θ_{int} = 0.8 mas.

Asteroseismic measurements of surface gravity were made for one more star of our sample, HD 49933 (Kallinger et al. 2010). They resulted in log g_{seis} = 4.22, which is only $1.4\sigma_g$ higher, than our value.

Spectroscopic stellar parameters were determined in a number of recent studies. We selected three of them for comparison. Bensby et al. (2014) used lines of Fe I and Fe II to derive temperatures and gravities of the extended stellar sample. The LTE abundances from individual lines were corrected using the grid of the NLTE abundance corrections from Lind et al. (2012). For nearby stars with very good HIPPARCOS parallaxes, Bensby et al. (2014) calculated also the log g_{Hip} values and found systematic discrepancies between the surface gravities from the two methods for the stars with log g > 4.2 and $T_{\rm eff}$ < 5650 K. Therefore, they applied empirical corrections to the atmospheric parameters from ionization balance. It should be reminded, we obtained no temperature trend of Δlog g(Sp – Hip) for our program stars (Sect. 5). Figure 14 (top panel) shows the differences in $T_{\rm eff}$ and log g for 17 stars in common with Bensby et al. (2014). On average, $\Delta T_{\rm eff} = -34 \pm 87$ K, Δlog g = −0.02±0.11, and Δ[Fe/H] = −0.02±0.11 in the sense "this work minus Bensby". The two independent

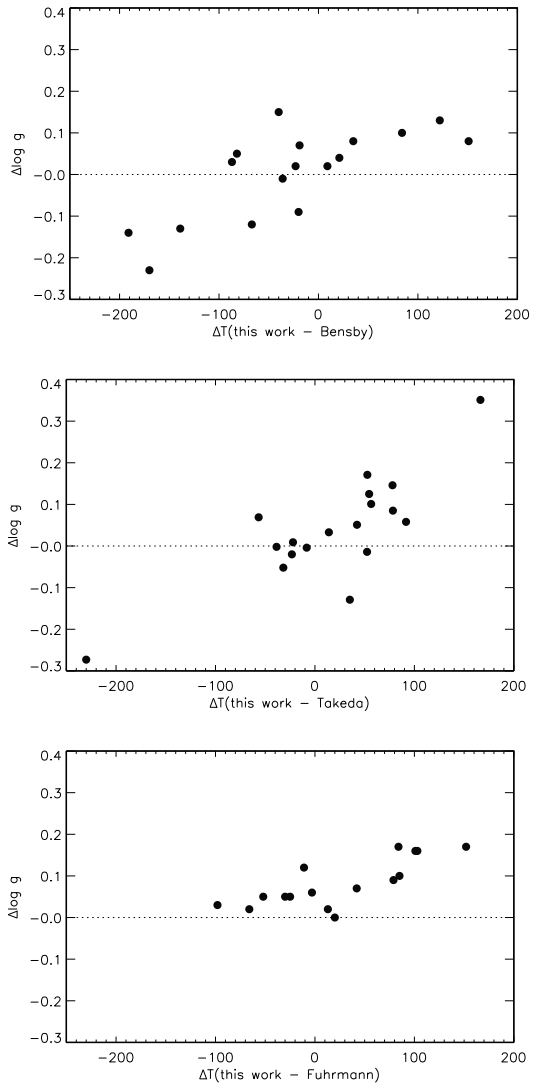

FIG. 14.— Differences in effective temperature and surface gravity between this study and the spectroscopic determinations by Bensby et al. (2014) (top panel), Takeda et al. (2005) (middle panel), and Fuhrmann (1998, 2004) (bottom panel).

research provide consistent stellar parameters, with the small systematic shifts and the statistical errors being typical of stellar parameter determinations. However, for some individual stars the discrepancies are uncomfortably large. For example, $\Delta T_{\rm eff}$ exceeds 100 K for five stars and $\Delta\log g > 0.2$ for HD 22879. We note, in particular, the differences of different sign for two well-studied very metal-poor stars HD 84937 and HD 140283, with $\Delta T_{\rm eff} = -190$ K and +120 K and $\Delta\log g = -0.14$ and +0.13, respectively. This can be due to large uncertainty in evaluating a slope of the log A(Fe I) versus $E_{\rm exc}$ trend, where the total number of investigated lines is limited. Since the Fe I/Fe II ionization equilibruim depends on not only surface gravity, but also $T_{\rm eff}$, an overestimation (underestimation) of $T_{\rm eff}$ produces an upward (downward) shift in log g.

Takeda et al. (2005) derived stellar $T_{\rm eff}$ and log g from lines of Fe I and Fe II under the LTE assumption. However, all the 18 stars in common with our work lie in the $-1.3 \leq$ [Fe/H] ≤ 0.2 metallicity range, where the departures from LTE for Fe I and Fe II are small. Therefore, the obtained differences in $T_{\rm eff}$ and log g (Fig. 14, middle panel) cannot be caused by applying different line-formation treatments. The data in Fig. 14 suggest, most probably, that the uncertainty in the derived effective temperature was directly translated to the uncertainty in surface gravity.

Fuhrmann (1998, 2004) applied different spectroscopic approaches to derive $T_{\rm eff}$ from the Balmer line wing fits and log g from the Mg Ib line profile fits under the LTE assumption. For 16 stars in common with this work, the mean differences in effective temperature and iron abundance, $\Delta T_{\rm eff} = 29 \pm 71$ K (Fig. 14, bottom panel) and Δ[Fe/H] $= 0.00 \pm 0.07$, do not exceed the error bars. The only star, HD 30743, was found with $\Delta T_{\rm eff} > 100$ K. However, this study obtains higher surface gravities, with $\Delta\log g = 0.08 \pm 0.07$. The discrepancy can be explained, in part, by using the LTE approach in Fuhrmann (1998, 2004). In the stellar parameter range, with which we concern, Mg I is subject to overionization resulting in weakened Mg Ib line. Ignoring the departures from LTE leads to an underestimation of the derived gravity.

7. CONCLUSIONS

The sample of 51 nearby FG dwarf stars uniformly distributed over the $-2.60 <$ [Fe/H] $< +0.20$ metallicity range was selected for a systematic NLTE investigation of the Galaxy chemical evolution. A membership of individual stars to the particular galactic stellar population, namely the thin disk, the thick disk, and the halo, was mainly identified using the star's kinematics and for few stars using also the chemical signatures, [Fe/H] and [Mg/Fe]. A combination of the photometric and spectroscopic methods was applied to derive a homogeneous set of the stellar atmosphere parameters: $T_{\rm eff}$, log g, [Fe/H], and ξ_t. Our spectroscopic analyses took advantage of employing the high-resolution ($R \geq 60\,000$) observed spectra and NLTE line formation for Fe I and Fe II in the classical 1D model atmospheres. Spectroscopic method of $T_{\rm eff}$/log g determination was tested using the 20 benchmark stars, for which there are multiple measurements of the IRFM effective temperature and their Hipparcos parallax error is less than 10 %. An efficiency of poorly known inelastic Fe+H collisions in the SE of Fe I-Fe II was estimated empirically from analysis of their different influence on lines of Fe I and Fe II in the MP benchmark stars. We found abundances from the two ionisation stages to be consistent within 0.06 dex for every star, when applying $S_{\rm H} = 0.5$.

Stellar parameters of the remaining 31 stars were obtained spectroscopically from the NLTE analysis of the iron lines. For lines of Fe II in our program stars the NLTE abundance corrections do not exceed 0.01 dex in absolute value. The deviations from LTE for Fe I grow towards higher $T_{\rm eff}$ and lower [Fe/H] and log g. For stars with either [Fe/H] ≥ -0.75, or $T_{\rm eff} \leq 5750$ K, or log g $\geq$ 4.20, the difference in average abundance between NLTE and LTE was found to be less than 0.06 dex, which translates to a shift of less than 0.1 dex in log g. Since NLTE leads to weakened lines of Fe I, but it does not affect lines of Fe II until the extremely low metallicities, the ionization equilibrium Fe I/Fe II is achieved for higher gravities in NLTE than in LTE. The NLTE analysis is crucial for the VMP turn-off and subgiant stars. Indeed, the shift in log g between NLTE and LTE reaches +0.45 dex for

BD−13° 3442, with $T_{\rm eff}$ = 6400 K, log g(NLTE) = 3.95, and [Fe/H] = −2.62.

The obtained effective temperatures and surface gravities were checked by comparing the star's position in the log g – $T_{\rm eff}$ plane with the theoretical evolutionary track of given metallicity and α-enhancement in the Yi et al. (2004) grid. Most stars reveal self-consistent data on star's mass, age, and kinematics.

Our final effective temperatures lie exactly in between the $T_{\rm IRFM}$ scales of A96 and C11, with a systematic shift of +46 K and −51 K, respectively. We estimate the $T_{\rm eff}$ statistical error to be about 70 K. Surface gravities obtained from the Fe I/Fe II and Hipparcos parallax methods were found to agree well. We do not confirm a temperature trend of Δlog g(Sp – Hip) reported by Bensby et al. (2014) for the log g > 4.2 and $T_{\rm eff}$ < 5650 K stars.

We recommend to apply a line-by-line differential approach relative to the Sun, to minimise the effect of the uncertainty in gf-values on the final results. It is quite efficient for the [Fe/H]> −1.5 stars. However, in the more metal-poor stars, the line-to-line scatter for Fe I has a similar magnitude for the differential and absolute abundances. This is, probably, due to uncertainties in C_6-values for the high-excitation lines. We note, in particular, Fe I 5367Å ($E_{\rm exc}$ = 4.41 eV) and Fe I 5383 Å ($E_{\rm exc}$ = 4.31 eV).

It was found that none of checked spectroscopic temperature indicators, such as Fe I versus Fe II, C I versus CH, and the H_α line wings, do support interferometric effective temperatures of HD 103095, T_{int} = 4818 K ± 54 K (Creevey et al. 2012), and HD 140283, T_{int} = 5534 ± 103 K (Creevey et al. 2015). Both stars have rather small angular diameters, and their measurements can be affected by some systematic trends, as suspected by Casagrande et al. (2014) for the Boyajian et al. (2012) dataset.

We conclude that the NLTE analysis of lines of iron in the two ionisation stages, Fe I and Fe II, is efficient in deriving reliable atmospheric parameters for the FG-type dwarf stars in the broad metallicity range, down to [Fe/H] = −2.6. The stellar parameter determinations would benefit from using the complementary data on interferometric and IRFM temperatures, trigonometric parallaxes, and asteroseismology measurements. We also recommend to combine different spectroscopic temperature and gravity indicators and check the obtained $T_{\rm eff}$/log g values with the theoretical evolutionary tracks / isochrones.

The obtained accurate atmospheric parameters will be used in the forthcoming papers to determine NLTE abundances of important astrophysical elements from lithium to europium and improve observational constraints on the chemo-dynamical models of the Galaxy evolution. We also plan to extend our sample toward lower metallicity and surface gravity.

The authors thank Prof. Debra Fisher for carrying out some of the observations, Oleg Kochukhov and Vadim Tsymbal for providing the codes binmag3 and synthV-NLTE at our disposal and Klaus Fuhrmann for providing the FOCES spectra. Y.Q. Chen acknowledges the observation of ESPaDOnS/CFHT telescope for two stars obtained through the Telescope Access Program (TAP, 2011B), which is funded by the National Astronomical Observatories. This study was supported by the Russian Foundation for Basic Research (grant 14-02-91153 and 14-02-31780), the National Natural Science Foundation of China (grants 11390371, 11233004, 11222326, 11103034, 11473033, 11473001), and by the National Basic Research Program of China (grant 2014CB845701/02/03). We made use the Simbad, MARCS, and VALD databases.

We thank the anonymous referee for comments that helped to improve the manuscript.

TABLE 2
Characteristics of observed spectra.

HD,BD	V	[Fe/H]	S/N	t_{exp}, s	N_{spec}	Date (yyyy-mm-dd)
			Shane/Hamilton			
19373	4.05	0.10	234, 228	30.00, 30.00	2	2012-01-09, 2012-01-09
22484	4.28	0.01	171, 160	30.00, 30.00	2	2012-01-09, 2012-01-09
22879	6.74	-0.84	170, 195	360.00, 360.00	2	2012-01-09, 2012-01-09
24289	9.96	-1.94	112, 128	2700.00, 2700.00	2	2012-01-09, 2012-01-09
30562	5.77	0.17	180, 190	120.00, 120.00	2	2012-01-09, 2012-01-09
30743	6.26	-0.44	188, 184	240.00, 240.00	2	2012-01-09, 2012-01-09
34411	4.70	0.01	220, 218, 209F[1]	45.00, 45.00, 84.19	3	2012-01-11, 2012-01-11, 2012-01-07
43318	5.65	-0.19	210, 212, 183F	100.00, 100.00, 215.14	3	2012-01-11, 2012-01-11, 2012-01-07
45067	5.90	-0.16	230, 235	180.00, 180.00	2	2012-01-09, 2012-01-09
45205	8.00	-0.87	140, 177	1200.00, 1800.00	2	2012-01-09, 2012-01-09
49933	5.78	-0.47	216, 203	659.71, 135.0	2	2012-01-08, 2012-01-10
52711	5.93	-0.21	256, 163F	160.00, 119.18	2	2012-01-10,2012-01-06
58855	5.36	-0.29	224, 167F	150.00, 75.13	2	2012-01-09, 2012-01-06
59374	8.50	-0.88	122F, 131F	1174.47, 812.31	2	2012-01-07, 2012-01-06
59984	5.93	-0.69	182F, 165F	269.17, 229.17	2	2012-01-07, 2012-01-06
62301	6.75	-0.70	197, 158F	450.00, 238.20	2	2012-01-09, 2012-01-06
64090	8.30	-1.73	280, 136F	2500.00, 687.35	2	2012-12-26, 2012-01-06
69897	5.10	-0.25	186, 180F	240.00, 66.18	2	2012-01-08, 2012-01-06
74000	9.67	-1.97	144, 142, 74F	2400.00, 2400.00, 1454.51	3	2012-01-10, 2012-01-10, 2012-01-06
76932	5.86	-0.98	170, 181F, 210F	612.32, 258.23, 489.24	3	2012-01-08, 2012-01-06, 2012-01-07
82943	6.54	0.19	214, 170F	270.00, 342.25	2	2012-01-10, 2012-01-06
84937	8.28	-2.16	122, 153, 95	1475.81, 1800.0, 846.41	3	2012-01-08, 2012-01-09, 2012-01-06
89744	5.74	0.13	220, 165F	135.00, 121.16	2	2012-01-10, 2012-01-06
90839	4.83	-0.18	190, 169F	60.00, 137.20	2	2012-01-10, 2012-01-06
92855	7.28	-0.12	171, 163F	600.00, 309.20	2	2012-01-10, 2012-01-06
94028	8.23	-1.47	118, 172	1800.00, 1317.69	2	2011-03-15, 2011-03-15
99984	5.95	-0.38	181F, 183F	517.22, 491.24	2	2012-01-07, 2012-01-07
100563	5.70	0.06	171F, 173F	413.25, 383.21	2	2012-01-07, 2012-01-07
102870	3.61	0.11	208F, 211F	77.12, 91.13	2	2012-01-07, 2012-01-07
103095	6.45	-1.26	188	300.00	1	2012-01-10
105755	8.59	-0.73	175, 103F	2400.0, 1052.44	2	2012-01-10, 2012-01-06
106516	6.11	-0.73	151F, 155F	434.25, 546.25	2	2012-01-07, 2012-01-07
108177	9.66	-1.67	60, 111	3000.00, 3600.00	2	2011-03-15, 2011-03-15
110897	6.00	-0.57	260, 170F, 172F	600.00, 568.30, 508.23	3	2012-01-08, 2012-01-07, 2012-01-07
114710	4.26	0.06	184F, 186F	112.13, 129.15	2	2012-01-07, 2012-01-07
115617	4.74	-0.10	177, 170	160.00, 160.00	2	2012-01-08, 2012-01-08
134088	8.00	-0.80	130	1800.00	1	2011-03-15
134169	7.67	-0.78	214, 212	750.00, 750.00	2	2012-01-10, 2012-01-10
138776	8.72	0.24	211	1800.00	1	2012-01-11
142091	4.82	-0.07	277, 275	60.00, 60.00	2	2012-01-11, 2012-01-11
142373	4.62	-0.54	140, 147	240.00, 240.00	2	2012-01-08, 2012-01-08
−04°3208	9.99	-2.20	60, 66	1500.00, 2400.00	2	2012-01-08, 2012-01-08
−13°3442	10.37	-2.62	103, 102, 104, 102	2700.00, 2700.00, 2700.00, 2700.00	4	2012-01-09, 2012-01-09, 2012-01-09, 2012-01-09
+24°1676	10.80	-2.44	86, 90, 92, 92, 57F	2400.00, 2400.00, 2400.00, 2400.00, 1581.60	5	2012-01-11, 2012-01-11, 2012-01-11, 2012-01-11, 2012-01-06
+29°2091	10.22	-1.91	82, 121, 115, 120, 83F	2400.00, 2700.00, 2700.00, 2700.00, 1287.46	5	2012-01-08, 2012-01-10, 2012-01-10, 2012-01-10, 2012-01-06
+37°1458	8.92	-1.95	235, 105F	2500.00, 897.38	2	2012-01-10, 2012-01-06
+66°0268	9.88	-2.06	112, 110, 115	2400.00, 2400.00, 2400.00	3	2012-01-10, 2012-01-10, 2012-01-10
G090-003	10.50	-2.04	106, 120, 122, 66F	2700.00, 2700.00, 2700.00, 1181.44	4	2012-01-11, 2012-01-11, 2012-01-11, 2012-01-06
			CFHT/ESPaDOnS			
+07°4841	10.38	-1.46	152	1470	2	
+09°0352	10.17	-2.09	160	2400	2	
			FOCES			
22879	6.74	-0.84	200	900.00, 1800.00, 1800.00	3	1996-09-02, 1999-01-02, 1996-10-31
34411	4.70	0.01	200	1500.00, 1500.00	2	1999-08-21, 1998-12-27
84937	8.28	-2.16	200	3600.00, 3300.00	2	1999-03-01, 1999-03-01
94028	8.23	-1.47	200	2400.00, 2400.00	2	2000-01-17, 2000-01-17
103095	6.45	-1.26	200	900.00	1	2000-05-19
142373	4.62	-0.54	200	600.00, 600.00	2	1998-06-09, 1998-06-09
			Others			
49933[2]	4.15	-0.47	500			
140283[3]	7.21	-2.46	200			
−04°3208[3]	9.99	-2.20	200			

Note. — [1] F indicates the observations carried out by Debra Fischer, [2] 3.6-m/HARPS, [3] VLT/UVES.

TABLE 3
Stellar kinematics and membership to particular galactic stellar population.

HD, BD	X-8000 (pc)	Y (pc)	Z (pc)	U ($km\,s^{-1}$)	V ($km\,s^{-1}$)	W ($km\,s^{-1}$)	[Mg/Fe] NLTE	Stellar population
19373	10	-10	-1	-75.2	-16.1	21.5	0.00 ± 0.03	Thin disk
22484	10	0	-9	1.7	-15.5	-42.3	-0.05 ± 0.02	Thin disk
22879	20	0	-17	-109.9	-88.2	-41.3	0.30 ± 0.02	Thick disk
24289	160	30	-139	-116.7	-172.6	173.9	0.21 ± 0.04	Halo
30562	20	10	-13	-54.9	-72.0	-21.6	0.04 ± 0.05	Thin disk
30743	20	20	-18	24.8	-5.2	-22.5	0.08 ± 0.06	Thin disk
34411	10	0	0	-74.5	-35.4	4.4	-0.03 ± 0.03	Thin disk
43318	30	20	-5	47.0	1.2	-37.0	-0.05 ± 0.05	Thin disk
45067	30	20	-3	-16.5	-64.4	13.7	0.01 ± 0.04	Thin disk
45205	60	-30	26	-35.9	-89.5	17.0	0.39 ± 0.03	Thick disk
49933	30	20	0	25.7	-13.1	-9.2	0.16 ± 0.10	Thin disk
52711	20	0	5	-18.6	-77.8	-9.0	0.01 ± 0.05	Thin disk
58855	20	0	9	25.3	-15.4	-3.9	0.07 ± 0.03	Thin disk
59374	40	20	14	-48.5	-120.3	-9.8	0.30 ± 0.02	Thick disk
59984	20	20	3	8.0	-11.4	-21.2	0.10 ± 0.02	Thin disk
62301	30	0	16	-7.4	-110.0	-22.1	0.26 ± 0.03	Thick disk
64090	30	0	13	266.9	-227.6	-89.6	0.24 ± 0.04	Halo
69897	20	0	9	-23.9	-38.7	7.1	-0.01 ± 0.06	Thin disk
74000	60	110	34	216.8	-348.0	62.2	0.37 ± 0.03	Halo
76932	10	20	7	-49.1	-91.3	70.0	0.32 ± 0.05	Thick disk
82943	10	20	13	13.3	-13.5	-12.6	-0.05 ± 0.05	Thin disk
84937	40	30	52	205.0	-214.7	-7.9	0.21 ± 0.08	Halo
89744	20	0	33	-10.6	-29.9	-14.3	-0.02 ± 0.04	Thin disk
90839	10	0	10	-13.9	-1.8	2.4	0.02 ± 0.03	Thin disk
92855	20	0	32	-42.1	-22.4	-13.9	-0.02 ± 0.04	Thin disk
94028	20	10	42	-33.7	-129.3	13.5	0.35 ± 0.05	Thick disk
99984	20	-10	49	-6.4	11.0	-36.1	0.02 ± 0.03	Thin disk
100563	0	10	24	-14.5	-20.9	-9.8	-0.03 ± 0.03	Thin disk
102870	0	10	10	40.4	3.2	7.3	-0.02 ± 0.03	Thin disk
103095	0	0	9	278.3	-157.2	-14.8	0.24 ± 0.06	Halo
105755	30	-30	78	26.7	5.3	8.3	0.34 ± 0.08	Thin disk
106516	0	10	18	53.4	-73.4	-57.7	0.38 ± 0.04	Thick disk
108177	-20	50	99	126.7	-262.9	32.0	0.23 ± 0.04	Halo
110897	0	0	17	-41.7	7.0	75.3	0.18 ± 0.03	Thin disk
114710	0	0	9	-49.9	11.5	8.4	-0.07 ± 0.04	Thin disk
115617	0	0	6	-23.3	-47.8	-31.3	-0.10 ± 0.02	Thin disk
134088	-30	0	26	-25.6	-72.4	-68.7	0.36 ± 0.03	Thick disk
134169	-40	0	44	2.5	-3.3	-1.9	0.32 ± 0.02	Thin disk
138776	-50	0	45	6.4	-56.4	-5.0	0.02 ± 0.04	Thin disk
140283	-50	0	32	-249.0	-253.3	41.1	0.23 ± 0.03	Halo
142091	-10	-20	24	33.6	-40.7	-18.1	0.07 ± 0.05	Thin disk
142373	0	-10	12	-41.6	10.8	-68.3	0.18 ± 0.01	Thin disk
−04° 3208	-30	110	169	-123.5	-309.9	-120.2	0.21 ± 0.06	Halo
−13° 3442							0.23 ± 0.01	Halo
+07° 4841	-50	-150	-123	-224.4	-283.9	-55.3	0.43 ± 0.05	Halo
+09° 0352	120	-40	-120	-156.5	-176.9	97.7	0.45 ± 0.05	Halo
+24° 1676	360	90	126	166.8	-483.7	106.4	0.21 ± 0.06	Halo
+29° 2091	40	20	85	157.3	-345.9	88.4	0.34 ± 0.04	Halo
+37° 1458	150	-10	26	-280.3	-233.0	-26.0	0.38 ± 0.05	Halo
+66° 0268	40	-40	10	-181.0	-426.4	-73.1	0.15 ± 0.07	Halo
G090-003	820	90	332	10.4	-824.6	-192.4	0.25 ± 0.05	Halo

TABLE 4
Line data, iron NLTE and LTE abundances from an analysis of the solar spectrum, and equvalent widths (EW) of the solar lines.

λ, Å	$E_{\rm exc}$ (eV)	log gf	log C_6	log A NLTE	log A LTE	EW mÅ
Fe I						
4920.50	2.83	0.07	-30.51	-4.61	-4.61	466.0
5198.72	2.22	-2.14	-31.32	-4.52	-4.53	102.0
5217.40	3.21	-1.07	-30.37	-4.57	-4.57	130.3
5232.94	2.94	-0.06	-30.54	-4.68	-4.68	371.1
5236.20	4.19	-1.50	-31.32	-4.68	-4.69	33.7
5242.50	3.63	-0.97	-31.56	-4.47	-4.47	93.4
5281.79	3.04	-0.83	-30.53	-4.68	-4.69	163.6
5324.18	3.21	-0.10	-30.42	-4.54	-4.54	332.5
5367.47	4.41	0.44	-30.20	-4.78	-4.78	170.1
5379.58	3.69	-1.51	-31.56	-4.46	-4.47	64.1
5383.37	4.31	0.64	-30.37	-4.72	-4.72	220.5
5393.17	3.24	-0.72	-30.42	-4.60	-4.60	171.2
5491.83	4.19	-2.19	-31.33	-4.53	-4.54	14.5
5586.76	3.37	-0.10	-30.38	-4.58	-4.58	289.3
5662.52	4.18	-0.57	-30.52	-4.41	-4.42	105.7
5696.09	4.55	-1.72	-30.21	-4.68	-4.69	14.6
5705.46	4.30	-1.36	-30.47	-4.61	-4.62	41.2
5778.45	2.59	-3.44	-31.37	-4.60	-4.61	22.7
5855.08	4.61	-1.48	-30.21	-4.58	-4.59	24.4
5916.25	2.45	-2.99	-31.45	-4.43	-4.44	56.7
6065.49	2.61	-1.53	-31.41	-4.51	-4.52	132.1
6082.71	2.22	-3.57	-31.74	-4.55	-4.56	34.7
6151.62	2.18	-3.30	-31.58	-4.52	-4.53	51.1
6200.32	2.61	-2.44	-31.43	-4.47	-4.48	74.6
6213.43	2.22	-2.48	-31.58	-4.58	-4.59	86.0
6229.23	2.85	-2.80	-31.32	-4.65	-4.66	37.8
6252.55	2.40	-1.69	-31.52	-4.52	-4.53	135.4
6393.61	2.43	-1.43	-31.53	-4.63	-4.64	150.8
6411.65	3.65	-0.60	-30.38	-4.57	-4.57	154.7
6421.35	2.28	-2.03	-31.80	-4.56	-4.57	112.7
6518.37	2.83	-2.46	-31.37	-4.59	-4.60	64.0
Fe II						
4233.17	2.58	-1.97	-32.01	-4.64	-4.64	132.1
4508.29	2.84	-2.44	-32.00	-4.48	-4.48	93.0
4582.83	2.83	-3.18	-32.03	-4.54	-4.54	57.7
4620.52	2.82	-3.21	-32.02	-4.63	-4.63	53.9
4923.93	2.88	-1.26	-32.03	-4.69	-4.69	196.1
5018.44	2.88	-1.10	-32.04	-4.72	-4.72	219.1
5197.58	3.22	-2.22	-32.02	-4.58	-4.58	85.4
5264.81	3.22	-3.13	-32.01	-4.48	-4.48	49.2
5284.11	2.88	-3.11	-32.04	-4.57	-4.57	60.3
5325.55	3.21	-3.16	-32.03	-4.55	-4.55	45.2
5414.07	3.21	-3.58	-32.02	-4.52	-4.52	29.8
5425.26	3.20	-3.22	-32.04	-4.56	-4.56	43.4
5991.38	3.15	-3.55	-32.05	-4.58	-4.58	32.1
6239.95	3.89	-3.46	-32.00	-4.55	-4.55	13.2
6247.56	3.89	-2.30	-32.00	-4.58	-4.58	55.0
6369.46	2.89	-4.11	-32.06	-4.59	-4.59	20.7
6432.68	2.89	-3.57	-32.07	-4.56	-4.56	43.2
6456.38	3.90	-2.05	-32.00	-4.59	-4.59	66.9

Note. — gf-values are from Blackwell et al. (1979, 1982a,b); O'Brian et al. (1991), and Bard et al. (1991) for Fe I and from Meléndez & Barbuy (2009) for Fe II.

TABLE 5
Final stellar parameters.

HD, BD	$T_{\rm eff}$ K	log g	[Fe/H]	ξ_t km s^{-1}	mass $M_\odot$	Fe I - Fe II LTE	Fe I - Fe II NLTE	$N_{\rm FeI}$	$N_{\rm FeII}$
Benchmark stars									
19373	6045 ± 80	4.24 ±0.05	0.10 ±0.05	1.2	1.11	0.06 ±0.09	0.06 ±0.09	26	15
22484	6000 ±100	4.07 ±0.05	0.01 ±0.04	1.1	1.18	-0.02 ±0.07	0.00 ±0.07	27	16
22879	5800 ± 90	4.29 ±0.07	-0.84 ±0.07	1.0	0.75	-0.06 ±0.08	-0.03 ±0.08	23	14
30562	5900 ± 85	4.08 ±0.05	0.17 ±0.08	1.3	1.12	0.02 ±0.09	0.02 ±0.09	26	16
34411	5850 ±100	4.23 ±0.05	0.01 ±0.03	1.2	1.10	-0.01 ±0.05	-0.02 ±0.05	26	15
49933	6600 ± 80	4.15 ±0.05	-0.47 ±0.07	1.7	1.11	-0.05 ±0.08	-0.04 ±0.08	26	15
59374	5850 ± 55	4.38 ±0.09	-0.88 ±0.05	1.2	0.75	-0.06 ±0.09	-0.02 ±0.09	24	15
59984	5930 ±100	4.02 ±0.06	-0.69 ±0.07	1.4	0.89	-0.06 ±0.10	-0.06 ±0.10	23	18
64090	5400 ± 70	4.70 ±0.08	-1.73 ±0.07	0.7	0.62	-0.02 ±0.09	-0.02 ±0.09	22	11
69897	6240 ± 70	4.24 ±0.05	-0.25 ±0.04	1.4	1.15	-0.06 ±0.07	-0.04 ±0.07	28	15
84937	6350 ± 85	4.09 ±0.08	-2.12 ±0.07	1.7	0.76	-0.06 ±0.11	0.00 ±0.12	12	7
94028	5970 ±130	4.33 ±0.08	-1.47 ±0.04	1.3	0.70	-0.06 ±0.07	-0.04 ±0.07	20	15
102870	6170 ± 80	4.14 ±0.04	0.11 ±0.06	1.5	1.35	-0.03 ±0.07	-0.01 ±0.07	23	14
103095	5130 ± 65	4.66 ±0.08	-1.26 ±0.08	0.9	0.60	0.01 ±0.11	0.01 ±0.11	22	8
105755	5800 ± 55	4.05 ±0.09	-0.73 ±0.05	1.2	0.85	-0.01 ±0.06	0.00 ±0.06	23	15
114710	6090 ± 80	4.47 ±0.05	0.06 ±0.06	1.1	1.17	0.03 ±0.07	0.04 ±0.06	26	15
134169	5890 ± 80	4.02 ±0.07	-0.78 ±0.07	1.2	0.87	0.01 ±0.09	0.06 ±0.09	26	18
140283	5780 ± 55	3.70 ±0.07	-2.46 ±0.07	1.6	0.80	-0.06 ±0.09	-0.02 ±0.09	20	14
142091	4810 ± 65	3.12 ±0.06	-0.07 ±0.10	1.2	1.16	0.05 ±0.13	0.05 ±0.12	20	13
+66° 0268	5300 ± 80	4.72 ±0.11	-2.06 ±0.15	0.6	0.60	-0.03 ±0.16	-0.03 ±0.16	21	9
Stars with spectroscopic parameters									
24289	5980	3.71	-1.94 ±0.17	1.1	0.83	-0.10 ±0.19	-0.03 ±0.19	16	10
30743	6450	4.20	-0.44 ±0.07	1.8	1.08	-0.03 ±0.09	0.01 ±0.09	26	18
43318	6250	3.92	-0.19 ±0.08	1.7	1.26	-0.05 ±0.13	-0.01 ±0.09	28	15
45067	5960	3.94	-0.16 ±0.06	1.5	1.18	-0.03 ±0.07	-0.01 ±0.07	24	16
45205	5790	4.08	-0.87 ±0.03	1.1	0.82	-0.08 ±0.07	-0.05±0.07	23	16
52711	5900	4.33	-0.21 ±0.05	1.2	0.97	0.03 ±0.07	0.05 ±0.07	26	16
58855	6410	4.32	-0.29 ±0.05	1.6	1.15	-0.01 ±0.08	0.01 ±0.07	26	15
62301	5840	4.09	-0.70 ±0.04	1.3	0.85	-0.07 ±0.08	-0.04 ±0.08	29	16
74000	6225	4.13	-1.97 ±0.07	1.3	0.76	-0.08 ±0.10	-0.02 ±0.10	15	7
76932	5870	4.10	-0.98 ±0.05	1.3		-0.01 ±0.07	0.03 ±0.08	27	16
82943	5970	4.37	0.19 ±0.04	1.2	1.17	0.01 ±0.06	0.01 ±0.06	25	13
89744	6280	3.97	0.13 ±0.03	1.7	1.50	0.01 ±0.05	0.02 ±0.06	26	13
90839	6195	4.38	-0.18 ±0.05	1.4	1.10	0.04 ±0.07	0.06 ±0.07	28	17
92855	6020	4.36	-0.12 ±0.03	1.3	1.08	0.00 ±0.06	0.02 ±0.05	24	11
99984	6190	3.72	-0.38 ±0.04	1.8	1.33	-0.01 ±0.07	0.03 ±0.07	24	15
100563	6460	4.32	0.06 ±0.08	1.6	1.30	0.00 ±0.10	0.02 ±0.10	23	10
106516	6300	4.44	-0.73 ±0.06	1.5	0.95	-0.03 ±0.08	0.00 ±0.08	22	15
108177	6100	4.22	-1.67±0.05	1.1	0.72	-0.08 ±0.13	-0.06 ±0.14	16	5
110897	5920	4.41	-0.57 ±0.04	1.2	0.85	0.03 ±0.05	0.05 ±0.05	29	18
115617	5490	4.40	-0.10 ±0.05	1.1	0.93	-0.04 ±0.08	-0.05 ±0.08	26	13
134088	5730	4.46	-0.80 ±0.05	1.1	0.75	-0.02 ±0.07	0.00 ±0.07	25	15
138776	5650	4.30	0.24 ±0.05	1.3	0.93	0.02 ±0.10	0.00 ±0.10	21	11
142373	5830	3.96	-0.54 ±0.05	1.4	0.95	-0.02 ±0.07	-0.02 ±0.07	28	17
–4° 3208	6390	4.08	-2.20 ±0.09	1.4	0.77	-0.08 ±0.11	0.00 ±0.11	16	11
–13° 3442	6400	3.95	-2.62 ±0.09	1.4	0.79	-0.14 ±0.11	0.00 ±0.11	8	5
+7° 4841	6130	4.15	-1.46 ±0.05	1.3	0.79	0.00 ±0.09	0.02 ±0.08	21	17
+9° 0352	6150	4.25	-2.09 ±0.04	1.3	0.70	-0.01 ±0.07	0.03 ±0.07	15	6
+24° 1676	6210	3.90	-2.44 ±0.09	1.5	0.78	-0.06 ±0.12	0.04 ±0.12	12	5
+29° 2091	5860	4.67	-1.91 ±0.08	0.8	0.70	-0.05 ±0.10	-0.05 ±0.10	18	10
+37° 1458	5500	3.70	-1.95 ±0.09	1.0		-0.07 ±0.11	-0.05 ±0.11	21	14
G090-003	6010	3.90	-2.04 ±0.06	1.3	0.78	-0.06 ±0.10	-0.02 ±0.10	17	12

REFERENCES

Adibekyan, V. Z., et al. 2013, A&A, 554, A44
Alexeeva, S., & Mashonkina, L. 2015, MNRAS, 00, 0, in preparation
Allende Prieto, C., Barklem, P. S., Lambert, D. L., & Cunha, K. 2004, A&A, 420, 183
Alonso, A., Arribas, S., & Martinez-Roger, C. 1995, A&A, 297, 197
—. 1996a, A&AS, 117, 227
—. 1996b, A&A, 313, 873
Axer, M., Fuhrmann, K., & Gehren, T. 1994, A&A, 291, 895
Bagnulo, S., Jehin, E., Ledoux, C., Cabanac, R., Melo, C., Gilmozzi, R., & ESO Paranal Science Operations Team. 2003, The Messenger, 114, 10
Bard, A., Kock, A., & Kock, M. 1991, A&A, 248, 315
Barklem, P. S., & Aspelund-Johansson, J. 2005, A&A, 435, 373
Barklem, P. S., Piskunov, N., & O'Mara, B. J. 2000, Astron. and Astrophys. Suppl. Ser., 142, 467
Bensby, T., Alves-Brito, A., Oey, M. S., Yong, D., & Meléndez, J. 2010, A&A, 516, L13
Bensby, T., Feltzing, S., & Oey, M. S. 2014, A&A, 562, A71
Bergemann, M., Lind, K., Collet, R., Magic, Z., & Asplund, M. 2012, MNRAS, 427, 27
Blackwell, D. E., Ibbetson, P. A., Petford, A. D., & Shallis, M. J. 1979, MNRAS, 186, 633
Blackwell, D. E., Petford, A. D., Shallis, M. J., & Simmons, G. J. 1982a, MNRAS, 199, 43
Blackwell, D. E., Petford, A. D., & Simmons, G. J. 1982b, MNRAS, 201, 595
Bonifacio, P., et al. 2009, A&A, 501, 519

Boyajian, T. S., et al. 2012, ApJ, 746, 101
—. 2013, ApJ, 771, 40
Butler, K., & Giddings, J. 1985, Newsletter on the analysis of astronomical spectra, No. 9, University of London
Carney, B. W., Latham, D. W., Laird, J. B., Grant, C. E., & Morse, J. A. 2001, AJ, 122, 3419
Casagrande, L., Ramírez, I., Meléndez, J., Bessell, M., & Asplund, M. 2010, A&A, 512, A54
Casagrande, L., Schönrich, R., Asplund, M., Cassisi, S., Ramírez, I., Meléndez, J., Bensby, T., & Feltzing, S. 2011, A&A, 530, A138
Casagrande, L., et al. 2014, MNRAS, 439, 2060
Cayrel, R., van't Veer-Menneret, C., Allard, N. F., & Stehlé, C. 2011, A&A, 531, A83
Cayrel, R., et al. 2004, A&A, 416, 1117
Cayrel de Strobel, G., Soubiran, C., & Ralite, N. 2001, A&A, 373, 159
Chen, Y. Q., Nissen, P. E., & Zhao, G. 2004, A&A, 425, 697
Chen, Y. Q., Nissen, P. E., Zhao, G., Zhang, H. W., & Benoni, T. 2000, A&AS, 141, 491
Chiappini, C., Matteucci, F., & Romano, D. 2001, ApJ, 554, 1044
Collet, R., Asplund, M., & Trampedach, R. 2007, A&A, 469, 687
Creevey, O. L., et al. 2012, A&A, 545, A17
—. 2013, MNRAS, 431, 2419
—. 2015, A&A, 575, A26
De Silva, G. M., et al. 2015, ArXiv e-prints
Dehnen, W., & Binney, J. J. 1998, MNRAS, 298, 387
Deng, L.-C., et al. 2012, Research in Astronomy and Astrophysics, 12, 735
Dobrovolskas, V., Kučinskas, A., Steffen, M., Ludwig, H.-G., Prakapavičius, D., Klevas, J., Caffau, E., & Bonifacio, P. 2013, A&A, 559, A102
Dotter, A., Chaboyer, B., Jevremović, D., Kostov, V., Baron, E., & Ferguson, J. W. 2008, ApJS, 178, 89
Drawin, H.-W. 1968, Zeitschrift fur Physik, 211, 404
Drawin, H. W. 1969, Zeitschrift fur Physik, 225, 483
Edvardsson, B., Andersen, J., Gustafsson, B., Lambert, D. L., Nissen, P. E., & Tomkin, J. 1993, A&A, 275, 101
Frebel, A., Casey, A. R., Jacobson, H. R., & Yu, Q. 2013, ApJ, 769, 57
Fuhrmann, K. 1998, A&A, 338, 161
—. 2000, http://www.ing.iac.es/∼klaus/ (Paper II)
—. 2004, Astronomische Nachrichten, 325, 3
Gehren, T., Shi, J. R., Zhang, H. W., Zhao, G., & Korn, A. J. 2006, A&A, 451, 1065
Gilmore, G., et al. 2012, The Messenger, 147, 25
González Hernández, J. I., & Bonifacio, P. 2009, A&A, 497, 497
Gratton, R., Carretta, E., Matteucci, F., & Sneden, C. 1996, in Astronomical Society of the Pacific Conference Series, Vol. 92, Formation of the Galactic Halo...Inside and Out, ed. H. L. Morrison & A. Sarajedini, 307
Gustafsson, B., Edvardsson, B., Eriksson, K., Jorgensen, U. G., Nordlund, Å., & Plez, B. 2008, A&A, 486, 951
Johnson, D. R. H., & Soderblom, D. R. 1987, AJ, 93, 864
Kallinger, T., Gruberbauer, M., Guenther, D. B., Fossati, L., & Weiss, W. W. 2010, A&A, 510, A106
Kobayashi, C., Karakas, A. I., & Umeda, H. 2011, MNRAS, 414, 3231
Kochukhov, O. 2010, http://www.astro.uu.se/∼oleg/binmag.html
Kurucz, R. L. 2007, Robert L. Kurucz on-line database of observed and predicted atomic transitions
Kurucz, R. L., Furenlid, I., Brault, J., & Testerman, L. 1984, Solar flux atlas from 296 to 1300 nm (New Mexico: National Solar Observatory)
Lai, D. K., Bolte, M., Johnson, J. A., Lucatello, S., Heger, A., & Woosley, S. E. 2008, ApJ, 681, 1524
Lind, K., Bergemann, M., & Asplund, M. 2012, MNRAS, 427, 50
Malkin, Z. M. 2013, Astronomy Reports, 57, 128
Mashonkina, L., & Gehren, T. 2000, A&A, 364, 249
Mashonkina, L., Gehren, T., Shi, J.-R., Korn, A. J., & Grupp, F. 2011, A&A, 528, A87
Mashonkina, L., Gehren, T., Travaglio, C., & Borkova, T. 2003, A&A, 397, 275
Mashonkina, L., et al. 2008, A&A, 478, 529
McWilliam, A., Preston, G. W., Sneden, C., & Searle, L. 1995, AJ, 109, 2757
Meléndez, J., & Barbuy, B. 2009, A&A, 497, 611
Mishenina, T. V., Soubiran, C., Kovtyukh, V. V., & Korotin, S. A. 2004, A&A, 418, 551
North, J. R., et al. 2009, MNRAS, 393, 245
Nissen, P. E., 1981, A&A, 97, 145
O'Brian, T. R., Wickliffe, M. E., Lawler, J. E., Whaling, W., & Brault, J. W. 1991, Journal of the Optical Society of America B Optical Physics, 8, 1185
Olsen, E. H. 1983, A&AS, 54, 55
—. 1993, A&AS, 102, 89
Pakhomov, Y. V., & Zhao, G. 2013, AJ, 146, 97
Raassen, A. J. J., & Uylings, P. H. M. 1998, VizieR Online Data Catalog, 334, 300
Ramírez, I., Allende Prieto, C., & Lambert, D. L. 2013, ApJ, 764, 78
Ramírez, I., & Meléndez, J. 2005, ApJ, 626, 446
Randich, S., Gilmore, G., & Gaia-ESO Consortium. 2013, The Messenger, 154, 47
Reddy, B. E., Tomkin, J., Lambert, D. L., & Allende Prieto, C. 2003, MNRAS, 340, 304
Reetz, J. K. 1991, Diploma Thesis (Universität München)
Romano, D., Karakas, A. I., Tosi, M., & Matteucci, F. 2010, A&A, 522, A32
Ruchti, G. R., Bergemann, M., Serenelli, A., Casagrande, L., & Lind, K. 2013, MNRAS, 429, 126
Ryabchikova, T., Fossati, L., & Shulyak, D. 2009, A&A, 506, 203
Skrutskie, M. F., et al. 2006, AJ, 131, 1163
Smiljanic, R., et al. 2014, A&A, 570, A122
Steenbock, W., & Holweger, H. 1984, A&A, 130, 319
Takeda, Y. 1994, PASJ, 46, 53
Takeda, Y., Ohkubo, M., Sato, B., Kambe, E., & Sadakane, K. 2005, PASJ, 57, 27
Tsymbal, V. 1996, in Astronomical Society of the Pacific Conference Series, Vol. 108, M.A.S.S., Model Atmospheres and Spectrum Synthesis, ed. S. J. Adelman, F. Kupka, & W. W. Weiss, 198
Turon, C., et al. 1993, Bulletin d'Information du Centre de Donnees Stellaires, 43, 5
van Leeuwen, F. 2007, A&A, 474, 653
von Braun, K., et al. 2014, MNRAS, 438, 2413
Yi, S. K., Demarque, P., & Kim, Y.-C. 2004, Ap&SS, 291, 261
Zasowski, G., et al. 2013, AJ, 146, 81
Zhang, H. W., & Zhao, G. 2005, MNRAS, 364, 712
—. 2006, A&A, 449, 127